

Eigenstates and instabilities of chains with embedded defects

J. D'Ambroise

Department of Mathematics, Bard College, Annandale-on-Hudson, NY 12504, USA

P.G. Kevrekidis

Department of Mathematics and Statistics, University of Massachusetts, Amherst, Massachusetts 01003-4515, USA

S. Lepri

*CNR-Consiglio Nazionale delle Ricerche, Istituto dei Sistemi Complessi,
via Madonna del piano 10, I-50019 Sesto Fiorentino, Italy*

We consider the eigenvalue problem for one-dimensional linear Schrödinger lattices (tight-binding) with an embedded few-sites linear or nonlinear, Hamiltonian or non-conservative defect (an oligomer). Such a problem arises when considering scattering states in the presence of (generally complex) impurities as well as in the stability analysis of nonlinear waves. We describe a general approach based on a matching of solutions of the linear portions of the lattice at the location of the oligomer defect. As specific examples we discuss both linear and nonlinear, Hamiltonian and \mathcal{PT} -symmetric dimers and trimers. In the linear case, this approach provides us a handle for semi-analytically computing the spectrum [this amounts to the solution of a polynomial equation]. In the nonlinear case, it enables the computation of the linearization spectrum around the stationary solutions. The calculations showcase the oscillatory instabilities that strongly nonlinear states typically manifest.

We consider the time evolution of a quantum mechanical wave function as governed by the Schrödinger equation. The wave function is distributed spatially on a discrete one-dimensional lattice, i.e. a chain of nodes indexed by integers, so that the spatial derivatives are replaced by differences. The potential function is nonzero only at a few center sites on the lattice, representing either physical impurities or other obstacles such as an external field or a nonlinear material. Since the general solution of the zero potential problem is well-known, we begin by constructing it on the outer (left and right) portions of the lattice. Working our way toward the impurity sites using the restraints of the discrete Schrödinger equation, we find that appropriately defined portions of the outer solution must satisfy a polynomial equation. Our method is also applied to the (again) discrete but (now) nonlinear Schrödinger equation. Here known stationary solutions are acted upon by a time-dependent perturbation, and we find that appropriately defined portions of the perturbation must satisfy polynomial equations. The main point is to show that the polynomial conditions we derive accurately determine the dynamical stability of the solutions. The success of our method in tracking the associated linear and nonlinear spectra is presented throughout the linear and nonlinear cases. In order to demonstrate the generality of our approach we show examples using both real valued Hamiltonians and purely complex parity-time symmetric potentials.

I. INTRODUCTION

Linear lattices with embedded impurities have been considered to model many different physical systems. A familiar example is the case of mass defects in an otherwise pure harmonic crystal. In the context of the tight-binding description of electron transport, the nonlinear terms describe the strong interaction with local vibrations at the impurity site [1]. Models of the same type have been used to describe tunneling through a magnetic impurity connected to two perfect leads in the presence of a magnetic field [2]. Another wide domain of application is the one of nonlinear optics. The type of system thereby considered is an array of coupled waveguides consisting of (at least) two types of materials one linear and one of Kerr type, see e.g. [3]. Several problems have been addressed, ranging from the existence of localized solutions residing on the nonlinear portion (nonlinear impurity modes [4]) to the scattering and transmission of plane waves through it [5].

An important question concerns the spectral characteristics of the problem in the linear regime and the dynamical stability of the solutions in the nonlinear regime (i.e., when the embedded impurities are genuinely nonlinear). To the best of our knowledge no systematic study of such an important issue been presented in the literature. In Ref. [6] the continuum case of Nonlinear Schrödinger equation with a localized (δ -function) nonlinearity was considered. For discrete lattices, an analysis of a related problem, the nonlinear Fano effect, has been reported in [7] (see also references therein). Another related reference is [8] where a bifurcation analysis of an open chain with nonlinearity and disorder is performed.

The aim of the present paper is to formulate (in general) and to solve (in some specific cases) the spectral problem

for a discrete Schrödinger equation with N embedded defects (an N -site oligomer [9]). Equations of this type emerge in, at least, two interesting cases. The first is the one of linear chains with localized *complex* on-site potentials. The second one arises when considering the stability problem of complex (i.e. current carrying) scattering solutions of the discrete nonlinear Schrödinger equation [5]. Such solutions can be computed exactly by the transfer matrix method [5, 10–12] and linearization around them yields linear equations of the same type.

Our motivation to approach this issue is twofold. The first is to study the scattering problem by open systems possessing a \mathcal{PT} -symmetry [13–15]. This theme is rapidly evolving into a major area of research partly due to its providing an intriguing alternative set of non-Hermitian Hamiltonians with potentially real eigenvalues and partly due to its experimental realizations in the field of nonlinear optics, both in the case of dimers [16, 17] and even in that of whole lattices [18]. The second motivation stems from a recent study of non-reciprocal wave propagation through non-mirror symmetric nonlinear lattices [19]. These are a minimal model for a “wave diode”, namely for devices capable to selectively rectify wave energy through a nonlinear medium of propagation. Relevant applications arise for instance for phonon scattering at a nonlinear interface layer between two very dissimilar crystals [20], acoustic waves in sonic materials [21] or in the so-called all-optical diode for photonic applications [22].

The solution of infinite-dimensional problems like the above is technically more involved than a straightforward matrix diagonalization. Indeed, to solve the problem exactly one should impose the solution a definite plane wave form (with generally complex wave numbers) in the two semi-infinite linear parts of the chain. The matching of such waves through the oligomer portion reduces the infinite-dimensional problem to an homogeneous linear system of $2N$ equations, whose solvability condition, along with the dispersion relations, yields a set of nonlinear equations for the unknowns.

The details of this method will be presented for a linear \mathcal{PT} -symmetric case [13–15]. In the latter, the imposition of the parity (\mathcal{P} , associated with spatial reflection) and time-reversal (\mathcal{T} , associated with temporal reflection and also $i \rightarrow -i$) symmetries leads to an imaginary (growth/decay) part of the Schrödinger potential which is spatially odd. The relevant more general constraint, in fact, reads $V(x) = V^*(-x)$ (where \star stands for complex conjugation); i.e., the real part of the relevant potential needs to be even. This setting will be compared/contrasted to the Hamiltonian case, where the potential is real.

The paper is organized as follows. In section II, we will discuss the simplest case namely that of linear oligomers. Although simple, this case is useful to set the stage of the general methodology and to illustrate some basic features that will be useful throughout the rest of the paper. In section III, we turn to the nonlinear case. In each of these, we first present the relevant analysis and subsequently we corroborate it on the basis of numerical computations. Finally, in section IV, we present a summary of our findings and some potential directions for future study.

II. LINEAR CASE

In this section we present the strategy to compute the spectrum and eigenstates of a general linear problem where N -site complex defects are embedded in an otherwise homogeneous lattice. More precisely, we consider the dynamic evolution of a one-dimensional chain governed by the linear discrete Schrödinger equation

$$i\dot{\phi}_n - V_n\phi_n + \phi_{n+1} + \phi_{n-1} = 0 \quad (1)$$

where $\phi_n(t) \in \mathbb{C}$. The complex potential $V_n \in \mathbb{C}$ is zero everywhere except for $1 \leq n \leq N$ for some integer $N \geq 2$.

We look for solutions of the form $\phi_n(t) = a_n e^{i\omega t}$ so that (1) becomes the time-independent condition

$$a_{n+1} + a_{n-1} - (V_n + \omega)a_n = 0. \quad (2)$$

Note that a_n is complex as well.

A. Theoretical Analysis

Our goal is to present a strategy for the analytic computation of the eigenstates a_n and eigenvalues ω , assuming that V_n has been prescribed. First we begin with an observation which applies to the portions of the lattice on the left and right of the N central sites. The zero potential ($V_n = 0$) version of equation (2) has a general solution of the form $a_n = Ae^{i\kappa n} + Be^{-i\kappa n}$ for $A, B \in \mathbb{C}$ and $\kappa \in \mathbb{C}$ satisfying the dispersion relation $2 \cos(\kappa) = \omega$. Thus we begin with the ansatz

$$a_n = \begin{cases} Ae^{i\kappa n} + Be^{-i\kappa n} & n < 1 \\ Ce^{i\kappa n} + De^{-i\kappa n} & n > N \end{cases} \quad (3)$$

for $A, C, B, D \in \mathbb{C}$ and κ satisfying

$$\omega = z + \frac{1}{z} \quad (4)$$

where we use the shorthand notation $z = e^{i\kappa} \neq 0$. Imposing (3) and (4) is enough to satisfy (2) for all n except $n = 0, 1, \dots, N, N + 1$. Applying (3) to (2) with $n = 0, N + 1$ shows that the formula (3) is applicable at $n = 1, N$. Since in practice we deal with a finite length lattice we introduce indexing $n_0 \leq n \leq m_0$ for large magnitude integers $n_0 \ll 1$ and $m_0 \gg N$. Imposing [27] homogeneous Dirichlet boundary conditions $a_{n_0-1} = a_{m_0+1} = 0$ shows that $\nu = a_{n_0+1}/a_{n_0} = a_{m_0-1}/a_{m_0}$. Combining this with (3) gives $B = -Ae^{2i\kappa(n_0-1)}$ and $D = -Ce^{2i\kappa(m_0+1)}$. Thus we have

$$a_n = \begin{cases} Ac_n & n \leq 1 \\ Cd_n & n \geq N \end{cases} \quad (5)$$

for $c_n = z^n - z^{2n_0-2-n}$ and $d_n = z^n - z^{2m_0+2-n}$.

At this point the imposition of (5) and (4) is enough to satisfy all but the N equations in (2) with $n = 1, \dots, N$. In the following sections we outline strategies for completing the computation of a_n and ω in the cases of embedded few-site defects and apply the method to our \mathcal{PT} -symmetric or Hamiltonian oligomer.

1. Oligomer of length two

For $N = 2$ we examine the two equations (2) for $n = 1, 2$ which by (5) can be written as

$$P \begin{bmatrix} a_0 \\ a_1 \\ a_2 \\ a_3 \end{bmatrix} = PQ \begin{bmatrix} A \\ C \end{bmatrix} = 0 \quad \text{for} \quad P = \begin{bmatrix} 1 & -(V_1 + \omega) & 1 & 0 \\ 0 & 1 & -(V_2 + \omega) & 1 \end{bmatrix} \quad \text{and} \quad Q = \begin{bmatrix} c_0 & 0 \\ c_1 & 0 \\ 0 & d_2 \\ 0 & d_3 \end{bmatrix}. \quad (6)$$

In other words, we now have a 2×2 system with unknowns A, C and coefficient matrix PQ . Imposing zero determinant $\det(PQ) = 0$ gives a solvability condition, which by (4) amounts to requiring that allowable z are roots of a polynomial with coefficients in terms of V_n . For each root z one computes the corresponding A, C by the equation in (6) so that finally an eigenvalue ω and eigenvector a_n are known by (4) and (5). Note that roots $z = \pm 1$ correspond to $c_n = d_n = a_n = 0$ and should be disregarded so as to obtain non-trivial eigenvectors.

As an example, consider the special case $V_1 + V_2 = 0$. One can compute by hand that the determinant condition, when expressed in terms of a positive power polynomial, is

$$0 = z^{2(m_0-n_0)+6} + (V_1V_2 - 1)z^{2(m_0-n_0)+4} - V_1z^{2m_0+1} - V_1V_2z^{2m_0} - V_2z^{2m_0-1} - V_2z^{-2n_0+7} - V_1V_2z^{-2n_0+6} - V_1z^{-2n_0+5} + (V_1V_2 - 1)z^2 + 1 \quad (7)$$

for which $z = \pm 1$ are each double roots. This reduces the number of relevant roots of (7) to $2(m_0 - n_0 + 1) \equiv 2L$, twice the length of the lattice. One can easily show, using the symmetry of the coefficients in (7), that solutions of (7) occur in reciprocal pairs $z, \frac{1}{z}$. Combining this with (4) shows that our analytic computation indeed yields exactly L eigenvalues ω , counted with multiplicity.

2. Oligomer of length three or greater

For $N > 2$ the strategy is similar to that of the last section but involves an additional step. First focus on the $N - 2$ equations (2) for $n = 2, \dots, N - 1$ which we write as

$$\begin{bmatrix} 1 & -(V_2 + \omega) & 1 & & \\ & \ddots & \ddots & \ddots & \\ & & & & \ddots \\ & & & 1 & -(V_{N-1} + \omega) & 1 \end{bmatrix} \begin{bmatrix} a_1 \\ \vdots \\ a_N \end{bmatrix} = 0. \quad (8)$$

By moving a_1 in the first equation and a_N in the last equation to the right-hand-side, (8) can be written as a square $(N - 2) \times (N - 2)$ system with unknowns a_2, \dots, a_{N-1} that can be computed linearly in terms of a_1, a_N (under appropriate conditions of invertibility of the resulting coefficient matrix). For the case of $N = 3$, Eq. (8) is one equation which we solve for a_2 in terms of a_1, a_3 to obtain

$$a_2 = \frac{a_1 + a_3}{V_2 + \omega} \stackrel{\text{by (5)}}{=} \frac{c_1 A + d_3 C}{V_2 + \omega} \quad (9)$$

for $\omega \neq -V_2$.

Continuing with the $N = 3$ case, we use (5) and (9) to rewrite the two remaining equations in (2) with $n = 1, 3$ as

$$P \begin{bmatrix} a_0 \\ a_1 \\ a_2 \\ a_3 \\ a_4 \end{bmatrix} = PQ \begin{bmatrix} A \\ C \end{bmatrix} = 0 \quad \text{for} \quad P = \begin{bmatrix} 1 & -(V_1 + \omega) & 1 & 0 & 0 \\ 0 & 0 & 1 & -(V_3 + \omega) & 1 \end{bmatrix} \quad \text{and} \quad Q = \begin{bmatrix} c_0 & 0 \\ c_1 & 0 \\ \frac{c_1}{V_2 + \omega} & \frac{d_3}{V_2 + \omega} \\ 0 & d_3 \\ 0 & d_4 \end{bmatrix}. \quad (10)$$

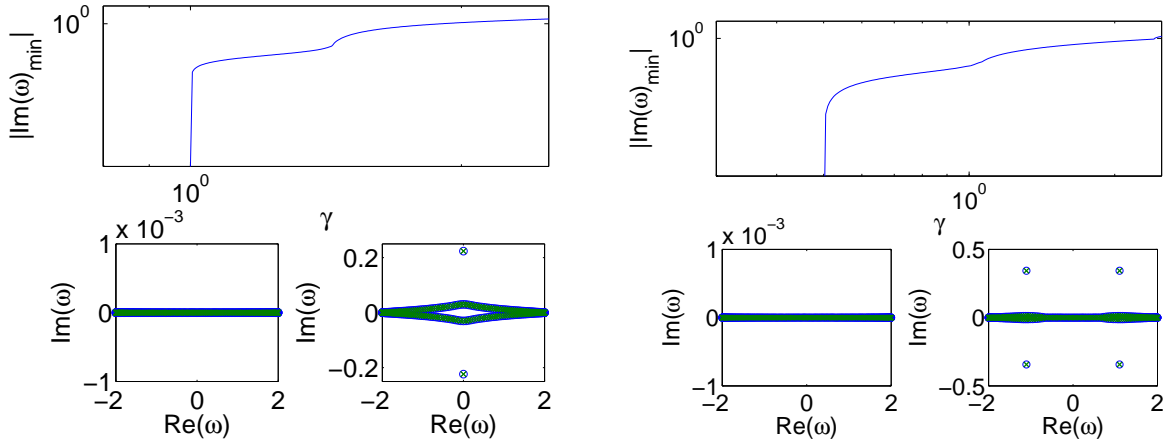


FIG. 1: The left set of panels corresponds to the linear \mathcal{PT} -symmetric dimer with $N = 2$, $\alpha_{1,2} = 0$ and $V_1 = i\gamma = -V_2$ while the right set of panels to the case of the trimer with $N = 3$, $\alpha_{1,2,3} = 0$ and $V_1 = i\gamma = -V_3$, $V_2 = 0$. Each set contains a (top) plot of linear stability eigenfrequencies as a function of increasing γ as computed on a lattice of length 200. The eigenvalue agreement between numeric (circles) and exact (x's) computations is shown for $\gamma = .5$ (bottom left) and $\gamma = 1.5$ (bottom right).

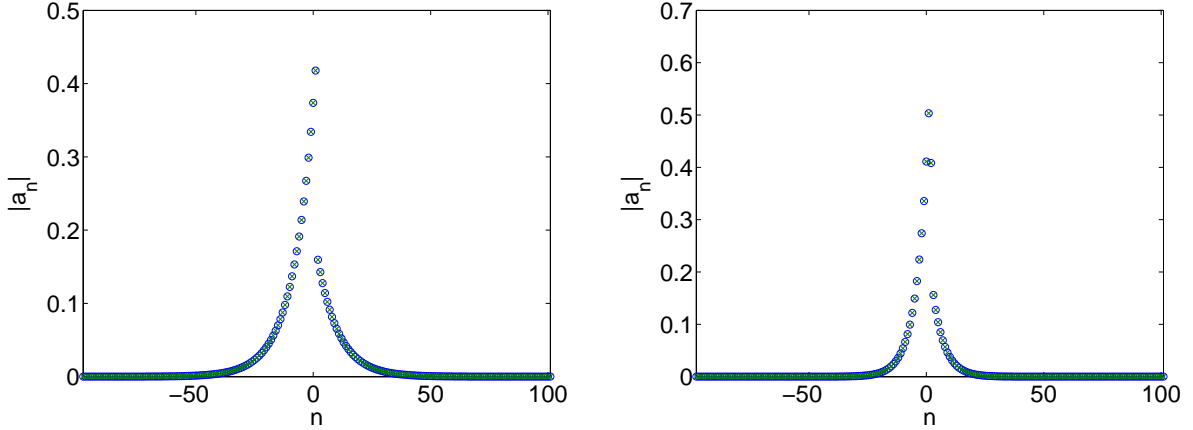


FIG. 2: Profiles of modulus of unstable eigenvectors $|a_n|$ are shown for the linear dimer (left) and the linear trimer (right). These eigenvectors correspond to the eigenvalues with negative imaginary part for $\gamma = 1.5$ which are seen in the bottom right panels of Fig. 1. Again, numerical computations (circles) are shown to agree with the exact computation (x's) and the lattice length is 200.

Again the solvability condition is $\det(PQ) = 0$ so that z is a root of a polynomial with coefficients in terms of V_n . For each z , one computes A, C in the nullspace of PQ from (10) so that by (4), (5) and (9), an eigenvalue ω and the corresponding eigenvector a_n are obtained. The $N > 3$ case is similar in that P and Q are determined using (5) and the above described process of using (8) to obtain expressions for a_2, \dots, a_{N-1} in terms of A, C .

Due to the condition obtained in (9), if there exists an eigenvalue $\omega = -V_2$ then it will not be found by the above process. In the case that such an eigenvalue exists the corresponding eigenvector is found by using (5) to rewrite the three $n = 1, 2, 3$ equations in (2) as the 2×2 system

$$\begin{bmatrix} (V_1 - V_2)c_1 - c_0 & (V_2 - V_3)d_3 + d_4 \\ c_1 & d_3 \end{bmatrix} \begin{bmatrix} A \\ C \end{bmatrix} = 0 \quad (11)$$

for z such that $z + \frac{1}{z} = -V_2$. Then a_n is computed by (5) and $a_2 = (V_1 - V_2)a_1 - a_0 = (V_3 - V_2)a_3 - a_4$.

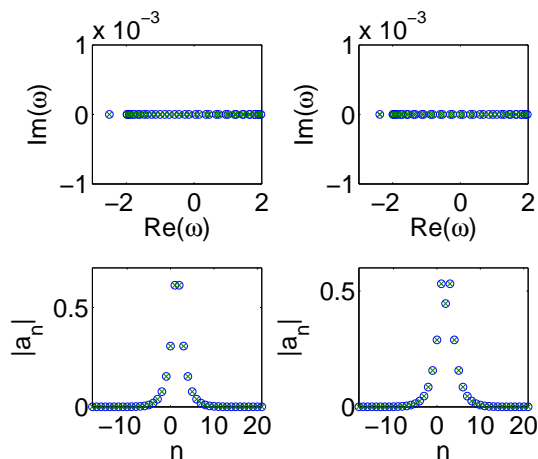


FIG. 3: The left set of plots corresponds to the linear Hamiltonian dimer with $N = 2$, $\alpha_{1,2} = 0$ and $V_1 = 1 = V_2$ while the right set of plots to the case of the linear trimer with $N = 3$, $\alpha_{1,2,3} = 0$ and $V_1 = 1 = V_3, V_2 = 0$. Each set contains a (top) plot of linear stability eigenvalues and a (bottom) plot of the eigenvector for the defect (point spectrum) mode. All plots show agreement between the numerical (circles) and semi-analytical (x's) results. Here the lattice length is 40.

B. Numerical results

First, we focus on the \mathcal{PT} -symmetric case where the dimer has linear potential $V_1 = -V_2 = i\gamma$ and the trimer potential is $V_1 = -V_3 = i\gamma$, while $V_2 = 0$. Fig. 1 shows agreement between the eigenvalues ω computed numerically directly from (2), through an eigenvalue solver, as compared to the semi-analytic calculation involving the identification of the roots of an equation of the form of Eq. (7), as outlined in the above theoretical analysis section. Fig. 2 shows the accuracy of the semi-analytic calculation in predicting the modulus profile of the eigenvectors $|a_n|$.

The spectra in Fig. 1 have both, as expected, a continuum component filling densely the interval $[-2, 2]$ on the real axis corresponding to the propagation of linear waves. For $\gamma > \gamma_c$ the solutions become unstable [28]; this is the so-called \mathcal{PT} -phase transition of [13–15]. In the case of the dimer, the principal unstable eigenfrequency pair has zero real part and is purely imaginary. In the case of the trimer, on the other hand, there is some oscillatory behaviour superimposed to the exponential growth of perturbations. The exponential localization of the associated eigenvectors is associated with the localized nature of the embedded defect structure and is showcased in Fig. 2.

Finally, as regards the linear eigenvalue problem, we consider the Hamiltonian case where the dimer has a linear potential $V_1 = V_0(1 + \delta)$, $V_2 = V_0(1 - \delta)$ and the trimer potential is $V_1 = V_0(1 + \delta)$, $V_2 = 0$, $V_3 = V_0(1 - \delta)$. Fig. 3 shows agreement between the numerically computed and semi-analytically calculated eigenvalues and the (modulus of the localized) eigenvectors. A fundamental difference here concerns the Hermitian nature of the relevant (matrix) operator which excludes the possibility of imaginary eigenfrequencies. Nevertheless, there exists within the spectrum a real defect eigenvalue. For $\delta > 0$, this frequency decreases as δ increases and the corresponding eigenvector profiles for $\delta > 0$ are typically similar to what is seen in Fig. 3.

III. NONLINEAR CASE

Let us now consider the nonlinear Schrödinger equation [23]

$$i\dot{\Phi}_n - V_n\Phi_n + \Phi_{n+1} + \Phi_{n-1} = \alpha_n|\Phi_n|^2\Phi_n \quad (12)$$

for $\alpha_n \in \mathbb{R}$ zero everywhere except $1 \leq n \leq N$. Seeking, as is customary, stationary solutions of the form $\Phi_n(t) = \psi_n e^{-i\omega t}$, we find that they should satisfy

$$\omega\psi_n - V_n\psi_n + \psi_{n+1} + \psi_{n-1} = \alpha_n|\psi_n|^2\psi_n. \quad (13)$$

We consider the dynamics of small perturbations defined by

$$\Phi_n(t) = (\psi_n + \epsilon\phi_n)e^{-i\omega t}; \quad \phi_n \equiv (a_n e^{i\nu t} + b_n e^{-i\nu^* t}) \quad (14)$$

for $\omega \in \mathbb{R}$ and $a_n, b_n, \nu \in \mathbb{C}$ and with $\psi_n \in \mathbb{C}$. In order to investigate the stability, we examine the resulting order- ϵ equations, amounting to the spectral or linear stability analysis equations

$$i\dot{\phi}_n = (V_n - \omega)\phi_n - \phi_{n+1} - \phi_{n-1} + \alpha_n(2|\psi_n|^2\phi_n + \psi_n^2\phi_n^*). \quad (15)$$

Note that ϕ_n is complex. It is thus recognized that problem (15) is similar to (1), the main difference being that now ϕ_n is coupled to ϕ_n^* . Hence, given a zeroth-order solution ψ_n , we can apply a similar approach as the one developed in section II, in order to determine its linearization spectrum.

For later reference, it is convenient to reformulate the problem in matrix form for a_n, b_n which are obtained from (12) by equating coefficients of $e^{i(\nu-\omega)t}, e^{-i(\nu^*+\omega)t}$, yielding

$$\nu \begin{bmatrix} a_n \\ b_n^* \end{bmatrix} = F \begin{bmatrix} a_n \\ b_n^* \end{bmatrix} \quad (16)$$

for $F = \begin{bmatrix} F_1 & F_2 \\ F_3 & F_4 \end{bmatrix}$ and

$$\begin{aligned} F_1 &= \text{diag}(\omega - V_n - 2\alpha_n |\psi_n|^2) + G & F_2 &= -\text{diag}(\alpha_n \psi_n^2) \\ F_3 &= \text{diag}(\alpha_n (\psi_n^*)^2) & F_4 &= -\text{diag}(\omega - V_n^* - 2\alpha_n |\psi_n|^2) - G \end{aligned} \quad (17)$$

where G is a sparse matrix with ones on the first super- and sub-diagonal.

A. Theoretical Analysis

Similar to the linear case we begin with the linearization problem ansatz

$$a_n = \begin{cases} Ae^{i\kappa n} + Be^{-i\kappa n} & n < 1 \\ Ce^{i\kappa n} + De^{-i\kappa n} & n > N \end{cases}, \quad b_n^* = \begin{cases} A'e^{i\kappa' n} + B'e^{-i\kappa' n} & n < 1 \\ C'e^{i\kappa' n} + D'e^{-i\kappa' n} & n > N \end{cases} \quad (18)$$

for $A, C, B, D, A', C', B', D' \in \mathbb{C}$ and $\kappa, \kappa' \in \mathbb{C}$ satisfying dispersion relations

$$\nu - \omega = 2 \cos(\kappa) \quad -(\nu + \omega) = 2 \cos(\kappa'). \quad (19)$$

Imposing (18) and (19) is enough to satisfy all equations in (16) except those with $n = 0, 1, \dots, N, N+1$. Applying (18) to (16) also shows that formulae (18) are applicable at $n = 1, N$. Homogeneous Dirichlet boundary conditions $a_{n_0-1} = b_{n_0-1}^* = a_{m_0+1} = b_{m_0+1}^* = 0$ (again for simplicity/specificity) imply that $\nu - \omega = a_{n_0+1}/a_{n_0} = a_{m_0-1}/a_{m_0}$ and $-(\nu + \omega) = b_{n_0+1}^*/b_{n_0}^* = b_{m_0-1}^*/b_{m_0}^*$ which when combined with the ansatz (18) gives $B = -Ae^{i\kappa(2n_0-2)}$, $D = -Ce^{i\kappa(2m_0+2)}$, $B' = -A'e^{i\kappa'(2n_0-2)}$, $D' = -C'e^{i\kappa'(2m_0+2)}$. Thus we have

$$a_n = \begin{cases} Ac_n & n \leq 1 \\ Cd_n & n \geq N \end{cases}, \quad b_n^* = \begin{cases} A'c'_n & n \leq 1 \\ C'd'_n & n \geq N \end{cases} \quad (20)$$

where c_n is defined in terms of $z = e^{i\kappa}$ as before and $c'_n = (z')^n - (z')^{2n_0-2-n}$, $d'_n = (z')^n - (z')^{2m_0+2-n}$ for $z' = e^{i\kappa'}$.

When combined with the dispersion relations (19), the condition (20) is enough to satisfy all except the $2N$ equations in (16) associated with $n = 1, \dots, N$. Again we separate the remaining parts of the computation into two sections.

1. Oligomer of length two

For $N = 2$ the remaining four equations in (16) for $n = 1, 2$ can be written as $Pv = 0$ for $P = \begin{pmatrix} P_1 & P_2 \\ P_3 & P_4 \end{pmatrix}$ and

$$\begin{aligned} P_1 &= \begin{bmatrix} 1 & \omega - \nu - V_1 - 2\alpha_1 |\psi_1|^2 & & 1 & & 0 \\ 0 & & 1 & & \omega - \nu - V_2 - 2\alpha_2 |\psi_2|^2 & 1 \end{bmatrix}, \quad P_2 = \begin{bmatrix} 0 & -\alpha_1 \psi_1^2 & 0 & 0 \\ 0 & 0 & -\alpha_2 \psi_2^2 & 0 \end{bmatrix}, \\ P_3 &= \begin{bmatrix} 0 & \alpha_1 (\psi_1^*)^2 & 0 & 0 \\ 0 & 0 & \alpha_2 (\psi_2^*)^2 & 0 \end{bmatrix}, \quad P_4 = \begin{bmatrix} -1 & -\omega - \nu + V_1^* + 2\alpha_1 |\psi_1|^2 & & -1 & & 0 \\ 0 & & -1 & & -\omega - \nu + V_2^* + 2\alpha_2 |\psi_2|^2 & -1 \end{bmatrix}, \end{aligned} \quad (21)$$

where $v = \begin{bmatrix} a_n \\ b_n^* \end{bmatrix}$ is a vector of length eight with each of a_n, b_n^* restricted to the index $0 \leq n \leq 3$. By (20), v can be written as

$$v = Q \begin{bmatrix} A \\ C \\ A' \\ C' \end{bmatrix} \quad \text{for} \quad Q = \begin{bmatrix} c_0 & 0 & 0 & 0 \\ c_1 & 0 & 0 & 0 \\ 0 & d_2 & 0 & 0 \\ 0 & d_3 & 0 & 0 \\ 0 & 0 & c'_0 & 0 \\ 0 & 0 & c'_1 & 0 \\ 0 & 0 & 0 & d'_2 \\ 0 & 0 & 0 & d'_3 \end{bmatrix}. \quad (22)$$

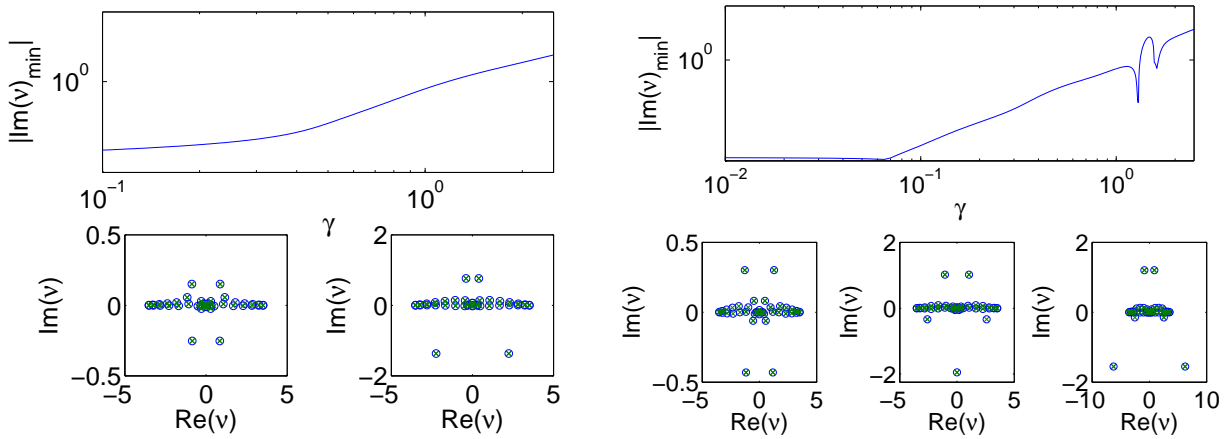


FIG. 4: The left set of panels corresponds to the \mathcal{PT} -symmetric dimer with $N = 2$, $\alpha_{1,2} = 1$ and $V_1 = i\gamma = -V_2$ while the right set of panels to the case of the trimer with $N = 3$, $\alpha_{1,2,3} = 1$ and $V_1 = i\gamma = -V_3, V_2 = 0$. Each set contains a (top) plot of linear stability eigenfrequencies of the stationary solution corresponding to $T = 0.7$ and $k_0 = 2.5$ as computed on a lattice of length 20. Plots of the eigenvalue ν indicating agreement between numeric (circles) and exact (x's) results are shown for the dimer with $\gamma = .5$ (bottom left) and $\gamma = 1.5$ (bottom right), and for the trimer with $\gamma = .5$ (bottom left) and $\gamma = 1.5$ (bottom middle) and $\gamma = 1.75$ (bottom right). For the trimer, when γ is small the dominant pair of (unstable) eigenfrequencies of negative imaginary part increases in magnitude as γ increases until $\gamma \approx 1.15$. At this point the complex pair recedes and a single dominant purely imaginary emerges. This single eigenfrequency increases in magnitude until $\gamma \approx 1.49$ when it begins to decrease. At $\gamma \approx 1.62$, a new dominant complex pair increases in magnitude and continues to increase as γ increases.

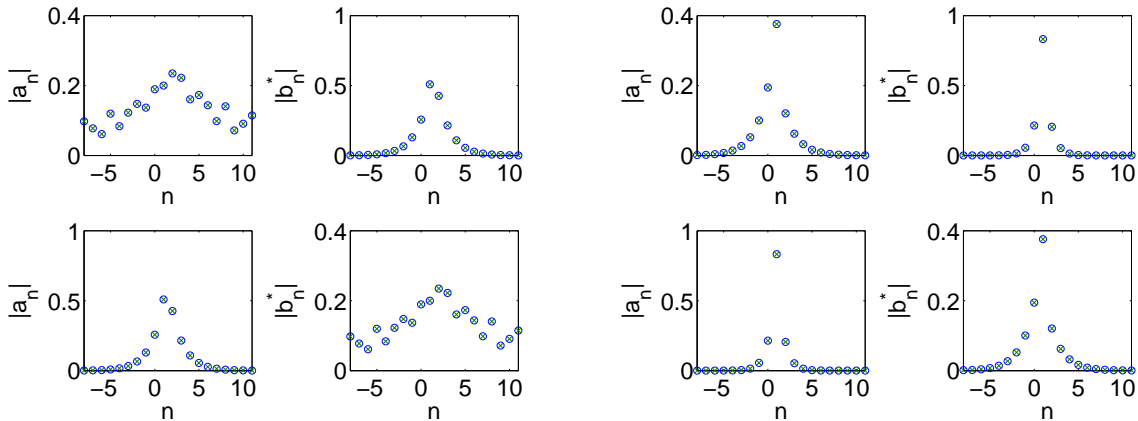


FIG. 5: Profiles of the moduli of unstable eigenvectors $|a_n|$, $|b_n^*|$ are shown for the nonlinear dimer. The left four plots show eigenvectors for $\gamma = .5$ and the right four plots for $\gamma = 1.5$. These eigenvectors correspond to eigenvalues with negative imaginary part which are seen in Fig. 4. Again, numerical computations are shown to agree with the exact (x's) results and the length of the lattice is 20. Notice the localization in both components of the eigenvector in the case of the \mathcal{PT} -symmetry breaking case of $\gamma > 1$.

The solvability condition is then the pair of equations

$$\det(PQ) = 0, \quad z + \frac{1}{z} + \omega = - \left(z' + \frac{1}{z'} + \omega \right) \quad (23)$$

where the second was obtained from the dispersion relations (19). Solutions of (23) where either of z or z' is ± 1 can be disregarded since the resulting system $Pv = 0$ has no non-trivial solutions. The remaining solutions appear in quadruple sets (z, z') , $(z, \frac{1}{z'})$, $(\frac{1}{z}, z')$, $(\frac{1}{z}, \frac{1}{z'})$ so that the total number of relevant solutions of (23) is four times the length of the lattice. Thus by (19) the calculation yields a number (counted with algebraic multiplicity) of eigenvalues ν equal to the length of the lattice.

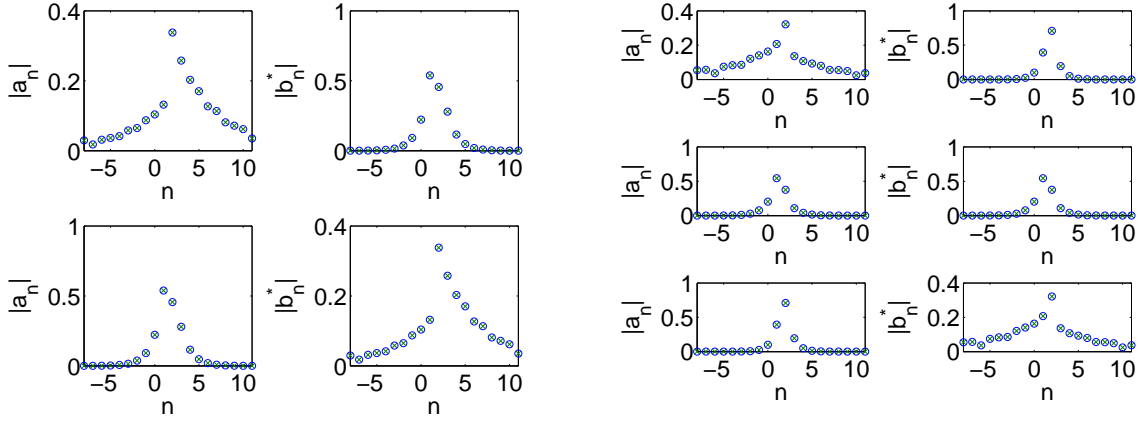


FIG. 6: Profiles of the moduli of unstable eigenvectors $|a_n|, |b_n^*|$ are shown for the nonlinear trimer with lattice length 20. The left four plots show eigenvectors for $\gamma = .5$ and the right six plots for $\gamma = 1.5$. These eigenvectors correspond to eigenvalues with negative imaginary part which are seen in Fig. 4. The agreement is similar to those of the earlier figures.

2. Oligomer of length three or greater

Similarly to the strategy for the linear case, for $N > 2$ we begin by examining the $2(N - 2)$ equations in (16) with $n = 2, \dots, N - 1$. Using (20) to rewrite the four quantities a_1, a_N, b_1^*, b_N^* one obtains a non-homogeneous square system where the $2(N - 2)$ variables $a_2, \dots, a_{N-1}, b_2^*, \dots, b_{N-1}^*$ can be computed as linear combinations of A, C, A', C' , under appropriate conditions of invertibility of the coefficient matrix.

In the case of $N = 3$ the $2(N - 2) = 2$ equations can be written as

$$\begin{bmatrix} 1 & \omega - \nu - V_2 - 2\alpha_2|\psi_2|^2 & 1 & 0 & -\alpha_2\psi_2^2 & 0 \\ 0 & \alpha_2(\psi_2^*)^2 & 0 & -1 & -\omega - \nu + V_2^* + 2\alpha_2|\psi_2|^2 & -1 \end{bmatrix} \begin{bmatrix} a_n \\ b_n^* \end{bmatrix} = 0 \quad (24)$$

where the column vector is length six with $1 \leq n \leq 3$. We move a_1, a_3, b_1^*, b_3^* to the right-hand-side of (24) and use (20) to obtain

$$\begin{bmatrix} a_2 \\ b_2^* \end{bmatrix} = M \begin{bmatrix} A \\ C \\ A' \\ C' \end{bmatrix} \quad \text{for} \quad M = \begin{bmatrix} \omega - \nu - V_2 - 2\alpha_2|\psi_2|^2 & -\alpha_2\psi_2^2 \\ \alpha_2(\psi_2^*)^2 & -\omega - \nu + V_2^* + 2\alpha_2|\psi_2|^2 \end{bmatrix}^{-1} \begin{bmatrix} -c_1 & -d_3 & 0 & 0 \\ 0 & 0 & c'_1 & d'_3 \end{bmatrix}. \quad (25)$$

Of course, (25) is the nonlinear analogue of (9) and the values of z which are found by the remaining parts of the computation are such that the inverse matrix in (25) exists. The four remaining equations in (16) with $n = 1, 3$ can now be written as $Pv = 0$ for $P = \begin{pmatrix} P_1 & P_2 \\ P_3 & P_4 \end{pmatrix}$ with

$$P_1 = \begin{bmatrix} 1 & \omega - \nu - V_1 - 2\alpha_1|\psi_1|^2 & 1 & 0 & 0 \\ 0 & 0 & 1 & \omega - \nu - V_3 - 2\alpha_3|\psi_3|^2 & 1 \end{bmatrix}, \quad P_2 = \begin{bmatrix} 0 & -\alpha_1\psi_1^2 & 0 & 0 & 0 \\ 0 & 0 & 0 & -\alpha_3\psi_3^2 & 0 \end{bmatrix} \quad (26)$$

$$P_3 = \begin{bmatrix} 0 & \alpha_1(\psi_1^*)^2 & 0 & 0 & 0 \\ 0 & 0 & 0 & \alpha_3(\psi_3^*)^2 & 0 \end{bmatrix}, \quad P_4 = \begin{bmatrix} -1 & -\omega - \nu + V_1^* + 2\alpha_1|\psi_1|^2 & -1 & 0 & 0 \\ 0 & 0 & 0 & -1 & -\omega - \nu + V_3^* + 2\alpha_3|\psi_3|^2 & -1 \end{bmatrix}$$

and where $v = \begin{bmatrix} a_n \\ b_n^* \end{bmatrix}$ is length ten with $0 \leq n \leq 4$. By (20) and (25) we write

$$v = Q \begin{bmatrix} A \\ C \\ A' \\ C' \end{bmatrix} \quad \text{for} \quad Q = \begin{bmatrix} c_0 & 0 & 0 & 0 \\ c_1 & 0 & 0 & 0 \\ M_{11} & M_{12} & M_{13} & M_{14} \\ 0 & d_3 & 0 & 0 \\ 0 & d_4 & 0 & 0 \\ 0 & 0 & c'_0 & 0 \\ 0 & 0 & c'_1 & 0 \\ M_{21} & M_{22} & M_{23} & M_{24} \\ 0 & 0 & 0 & d'_3 \\ 0 & 0 & 0 & d'_4 \end{bmatrix}. \quad (27)$$

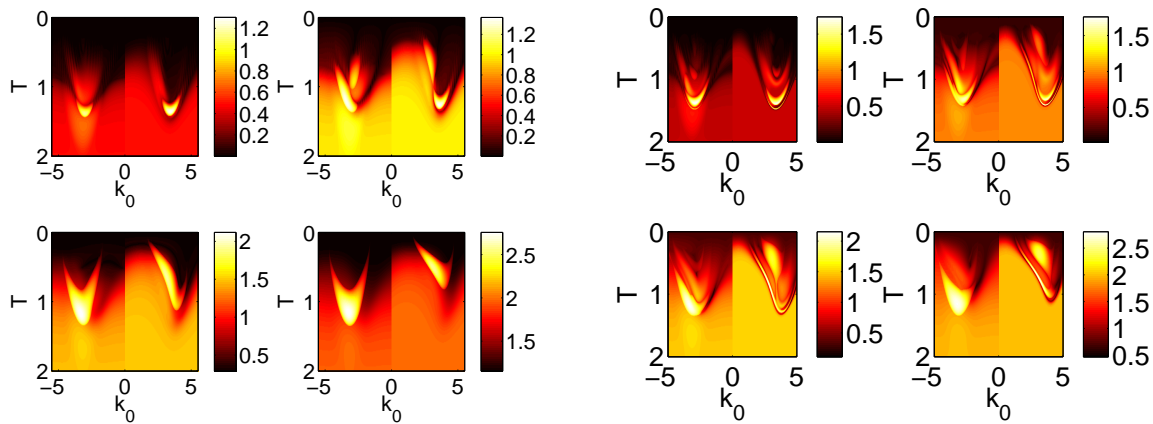


FIG. 7: The left set of panels correspond to the \mathcal{PT} -symmetric dimer with $N = 2$, $\alpha_{1,2} = 1$ and $V_1 = i\gamma = -V_2$ while the right set of panels to the case of the trimer with $N = 3$, $\alpha_{1,2,3} = 1$ and $V_1 = i\gamma = -V_3, V_2 = 0$. Each set contains contour plots of extremal stability eigenfrequencies $|Im(\nu)_{min}|$ for extended solutions as in (28) on a lattice of length 20 with $\gamma = .5$ (top left), $\gamma = 1$ (top right), $\gamma = 1.5$ (bottom left) and $\gamma = 2$ (bottom right).

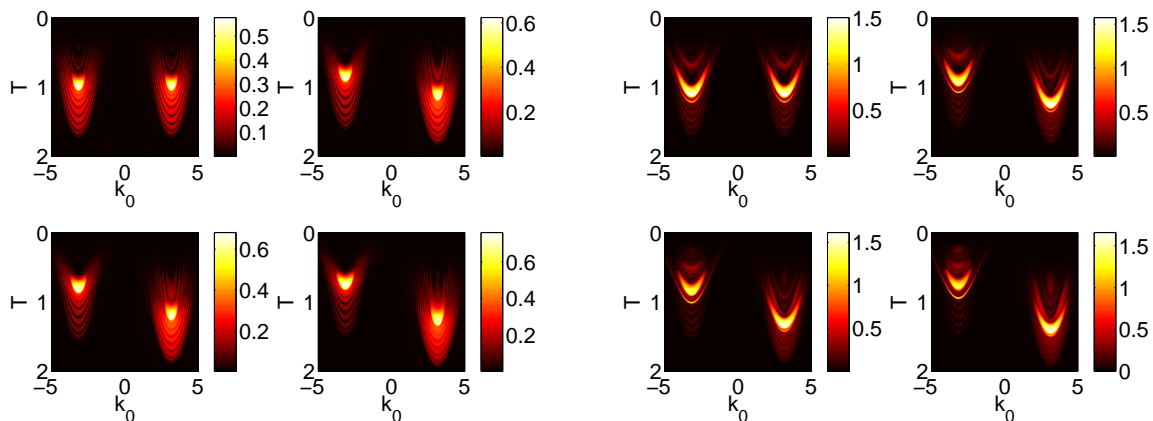


FIG. 8: The left set of panels correspond to the Hamiltonian dimer with $N = 2$, $\alpha_{1,2} = 1$ and $V_1 = 1 + \delta, V_2 = 1 - \delta$ while the right set of panels to the case of the trimer with $N = 3$, $\alpha_{1,2,3} = 1$ and $V_1 = 1 + \delta, V_2 = 0, V_3 = 1 - \delta$. Each set contains contour plots of extremal stability eigenfrequencies $|Im(\nu)_{min}|$ for extended solutions as in (28) on a lattice of length 20 with $\delta = 0$ (top left), $\delta = 0.5$ (top right), $\delta = 0.75$ (bottom left) and $\delta = 1$ (bottom right).

The solvability condition is the same as (23) but with P and Q as defined in (26) and (27), respectively. Again, solutions with either z or z' equal to ± 1 are not relevant.

B. Numerical results

As mentioned in the Introduction, one of the motivations of the present work is to study the stability of scattering solutions. In particular, we focus here on of the class of plane wave solutions of (13) of the form

$$\psi_n = \begin{cases} R_0 e^{ik_0 n} + R e^{-ik_0 n} & n \leq 1 \\ T e^{ik_0 n} & n \geq N \end{cases} \quad (28)$$

with $R_0, R, T \in \mathbb{C}$ representing the incident, reflected and transmitted amplitudes, respectively and $k_0 \geq 0$ is the wavenumber such that $\omega = -2 \cos(k_0)$. For each given values of k_0, T one can compute ψ_n by repeated application of the backwards transfer map [5, 10–12]

$$\psi_{n-1} = -\psi_{n+1} + (V_n - \omega + \alpha_n |\psi_n|^2) \psi_n \quad (29)$$

which is a rearrangement of (13). For short oligomers, like the ones we are dealing with here, the ψ_n can be evaluated analytically [19, 24].

Fig. 4 shows an example of the the eigenvalues ν computed with the method discussed in the previous section. As a check, we also report eigenvalues computed by numerical diagonalization of the matrix F in (16) evaluated by substituting the computed ψ_n in (17). The corresponding eigenvectors for the case of the dimer and the trimer are shown, respectively, in Figs. 5 and 6.

It is clear that past the critical point of the \mathcal{PT} phase transition, the relevant eigenvectors become highly localized (contrary to what is the case with the more spatially extended eigenvectors before the transition). These eigenvectors are responsible for the rapid growth of the norm density at the gain node observed previously [24]. The analysis also confirms the finding from our previous work [24] that higher values of γ and T correspond to more unstable solutions. We partially capture this phenomenon in Fig. 7, which contains a systematic two-parameter diagram of the dependence of the growth rate of the corresponding most unstable eigenstates. In addition to the stronger instability for higher T observed in the figure (and also for higher γ in Fig. 4), we observe the asymmetry of the relevant growth rate for transmission in the direction of positive vs. negative k_0 (as in [19, 24] we have adopted the convention that $-k_0$ labels a right-incoming solution with wavenumber k_0). Among these two directions, it is intuitively clear and numerically confirmed that larger growth rates are incurred for waves that first encounter the gain site. For a fixed γ , the transition from right-incoming ($-k_0 < 0$) to left-incoming ($k_0 > 0$) waves may be achieved computationally by allowing the wave number to stay positive and instead flipping the potential V_n from left to right. For the \mathcal{PT} case this amounts to a continuous change in k_0 and a discontinuous change in the fixed γ value from negative to positive. This explains the discontinuity apparent in Fig. 7.

Finally, we touch upon the Hamiltonian case namely the case of real-valued V_n for the nonlinear problem [19] [once again we use a dimer with $V_1 = V_0(1 + \delta)$, $V_2 = V_0(1 - \delta)$ and a trimer with $V_1 = V_0(1 + \delta)$, $V_2 = 0$, $V_3 = V_0(1 - \delta)$]. This is captured in Fig. 8. In the Hamiltonian case the instability for the dimer associated with the particular values $k_0 = 2.5$ and $T = 0.7$, for example, increases as δ increases from zero to $\delta \approx 1.35$ then the instability decreases for increasing δ . Additional oscillations appear in Figure 8 as an artifact of the short lattice length which we used to obtain the higher resolution with respect to the axes of Figure 8. These extra fluctuations disappear for the dimer as the length of the lattice becomes large. Nevertheless, the persistent characteristic corroborating the earlier work of [19] identified here concerns the asymmetry of transmission between incoming from the left ($k_0 > 0$) and from the right ($k_0 < 0$).

IV. CONCLUSIONS & FUTURE CHALLENGES

In this work, we have presented a methodology for addressing the spectral analysis of linear (or linearized) chains that possess an embedded oligomer defect. The technique, which draws a series of direct parallels with the approach used in [6], consists of the solution of the linear problem (with its boundary conditions) on the lattice in which the defect is embedded. Subsequently these two linear solutions (on the left and right of the defect) are used as boundary conditions of the embedded region. Nontrivial solutions require that the determinant of a suitably defined matrix vanishes, ultimately leading to a polynomial problem for the eigenvalue, of the form given by (23). Based on the solution of this resulting polynomial (which can be written fairly explicitly e.g. in the dimer case, see Eq. 7), we can obtain the eigenvalues and reconstruct the eigenvectors of the full problem.

We have applied the approach to genuinely linear problems with embedded complex oligomers, and, in the second part of the paper, to solve the stability problem as it arises from linearization around (analytically known or numerically computed) extended solutions with an embedded nonlinear defect. Finally, we calculated the spectrum and eigenstates in a number of cases of interest for \mathcal{PT} -symmetric and Hamiltonian potentials. Our semi-analytical approach shows excellent agreement with numeric computations of the spectrum.

The instabilities found in the nonlinear cases are generically oscillatory, with unstable eigenvalues having a non zero real and imaginary part and thus leading to oscillatory growth. The question, however, of the dynamical development of the instability and of the ultimate fate of such solutions is still in many respects open to more systematic studies. In the Hamiltonian case, there is numerical evidence that the instability leads to self-trapping of energy at the oligomer [25]. On the other hand, the dynamics of the \mathcal{PT} case is fundamentally different in the instability development, usually ending in an indefinite growth at the gain site [24].

An especially interesting direction would be to consider generalizations of the present problem to higher dimensional settings. A priori, the solution of the linear problem is available in this case as well, e.g. for a square defect. Yet the matching of the solutions from the four relevant directions in the two-dimensional case presents considerable challenges. Generalizing the approach for both linear and nonlinear problems in such a case would be a particularly interesting topic for future studies. Another interesting issue to examine, even in the one dimensional setting, is the effect of boundary size on the eigenvalues of the problem (especially, so the \mathcal{PT} -symmetric one). Both our earlier work [24] and that of others [26] have suggested interesting effects stemming from the finite size of the domain (and the associated boundary conditions) within which the embedded defect lies. Studying such effects and their scaling over the domain size would be another interesting direction for future work. Relevant themes are currently under

consideration and will be reported in future publications.

-
- [1] G.P. Tsironis, M.I. Molina and D. Hennig, *Phys. Rev. E* **50**, 2365 (1994).
- [2] M.I. Molina, H. Bahlouli *Phys. Lett. A* **284**, 87 (2002).
- [3] K. Hizanidis, Y. Kominis and N.K. Efremidis, *Opt. Express* **16**, 18296 (2008).
- [4] P. G. Kevrekidis, Yu. S. Kivshar, and A. S. Kovalev *Phys. Rev. E* **67**, 046604 (2003)
- [5] G.P. Tsironis and D. Hennig. *Phys. Rep.*, **307**, 333 (1999).
- [6] B. A. Malomed and M. Ya. Azbel. *Phys. Rev. B*, **47**, 10402–10406 (1993).
- [7] A. E. Miroshnichenko. *Phys. Lett. A*, **373**, 3586, (2009).
- [8] S. Tietsche and A. Pikovsky. *Europhys. Lett.*, **84**:10006 (2008).
- [9] K. Li and P. G. Kevrekidis *Phys. Rev. E* **83**, 066608 (2011)
- [10] F. Delyon, Y.E. Lévy, and B. Souillard, *Phys. Rev. Lett.*, **57**, 2010–2013 (1986).
- [11] Y. Wan and CM Soukoulis, *Phys. Rev. A*, **41**, 800–809 (1990).
- [12] Q. Li, CT Chan, K.M Ho, and C.M. Soukoulis, *Phys. Rev. B*, **53** 15577–15585, (1996).
- [13] C. M. Bender and S. Boettcher, *Phys. Rev. Lett.* **80**, 5243-5246 (1998).
- [14] C. M. Bender, S. Boettcher and P. N. Meisinger, *J. Math. Phys.* **40**, 2201-2209 (1999).
- [15] C. M. Bender, *Rep. Prog. Phys.* **70**, 947-1018 (2007).
- [16] A. Guo, G. J. Salamo, D. Duchesne, R. Morandotti, M. Volatier-Ravat, V. Aimez, G. A. Siviloglou, and D. N. Christodoulides, *Phys. Rev. Lett.* **103**, 093902 (2009).
- [17] C.E. Rüter, K.G. Makris, R. El-Ganainy, D.N. Christodoulides, M.Segev, and D. Kip, *Nature Physics* **6**, 192-195 (2010).
- [18] A. Regensburger, C. Bersch, M.-A. Miri, G. Onishchukov, D.N. Christodoulides and U. Peschel, *Nature* **488**, 167-171 (2012).
- [19] S. Lepri and G. Casati, *Phys. Rev. Lett.* **106**, 164101 (2011).
- [20] Yu. A. Kosevich, *Phys. Rev. B*, **52**, 1017 (1995).
- [21] N. Boechler, G. Theocharis and C. Daraio, *Nature Materials* **10**, 665 (2011).
- [22] M. Scalora, J. P. Dowling, C. M. Bowden, and M. J. Bloemer, *J. Appl. Phys.* **76**, 2023 (1994); M. D. Tocci, M. J. Bloemer, M. Scalora, J. P. Dowling, and C. M. Bowden, *Appl. Phys. Lett.* **66**, 2324 (1995).
- [23] P. G. Kevrekidis. *The Discrete Nonlinear Schrödinger Equation*. Springer Verlag, Berlin, 2009.
- [24] J. D’Ambrose, P.G. Kevrekidis, and S. Lepri. *J. Phys. A* **45**, 444012 (2012).
- [25] S. Lepri and G. Casati, unpublished.
- [26] A.A. Sukhorukov, S.V. Dmitriev, S.V. Suchkov and Yu.S. Kivshar, *Opt. Lett.* **37**, 2148 (2012).
- [27] This imposition is for simplicity/specificity of the calculation; other boundary conditions can be treated in similar ways by applying them to the solution of Eq. (3), to obtain two conditions relating A , B , C and D .
- [28] It should be noted that $\gamma_c = 1$ for the pure dimer (not embedded on a lattice) and for the dimer embedded on a finite lattice. Remarkably, the case of a dimer embedded in the infinite lattice has a different $\gamma_c = \sqrt{2}$ (D.E. Pelinovsky, personal communication). However, as our aim herein is to analyze the finite lattice case, we do not focus on this aspect further in what follows.

Eigenstates and instabilities of chains with embedded defects

J. D'Ambroise

Department of Mathematics, Bard College, Annandale-on-Hudson, NY 12504, USA

P.G. Kevrekidis

Department of Mathematics and Statistics, University of Massachusetts, Amherst, Massachusetts 01003-4515, USA

S. Lepri

*CNR-Consiglio Nazionale delle Ricerche, Istituto dei Sistemi Complessi,
via Madonna del piano 10, I-50019 Sesto Fiorentino, Italy*

We consider the eigenvalue problem for one-dimensional linear Schrödinger lattices (tight-binding) with an embedded few-sites linear or nonlinear, Hamiltonian or non-conservative defect (an oligomer). Such a problem arises when considering scattering states in the presence of (generally complex) impurities as well as in the stability analysis of nonlinear waves. We describe a general approach based on a matching of solutions of the linear portions of the lattice at the location of the oligomer defect. As specific examples we discuss both linear and nonlinear, Hamiltonian and \mathcal{PT} -symmetric dimers and trimers. In the linear case, this approach provides us a handle for semi-analytically computing the spectrum [this amounts to the solution of a polynomial equation]. In the nonlinear case, it enables the computation of the linearization spectrum around the stationary solutions. The calculations showcase the oscillatory instabilities that strongly nonlinear states typically manifest.

We consider the time evolution of a quantum mechanical wave function as governed by the Schrödinger equation. The wave function is distributed spatially on a discrete one-dimensional lattice, i.e. a chain of nodes indexed by integers, so that the spatial derivatives are replaced by differences. The potential function is nonzero only at a few center sites on the lattice, representing either physical impurities or other obstacles such as an external field or a nonlinear material. Since the general solution of the zero potential problem is well-known, we begin by constructing it on the outer (left and right) portions of the lattice. Working our way toward the impurity sites using the restraints of the discrete Schrödinger equation, we find that appropriately defined portions of the outer solution must satisfy a polynomial equation. Our method is also applied to the (again) discrete but (now) nonlinear Schrödinger equation. Here known stationary solutions are acted upon by a time-dependent perturbation, and we find that appropriately defined portions of the perturbation must satisfy polynomial equations. The main point is to show that the polynomial conditions we derive accurately determine the dynamical stability of the solutions. The success of our method in tracking the associated linear and nonlinear spectra is presented throughout the linear and nonlinear cases. In order to demonstrate the generality of our approach we show examples using both real valued Hamiltonians and purely complex parity-time symmetric potentials.

I. INTRODUCTION

Linear lattices with embedded impurities have been considered to model many different physical systems. A familiar example is the case of mass defects in an otherwise pure harmonic crystal. In the context of the tight-binding description of electron transport, the nonlinear terms describe the strong interaction with local vibrations at the impurity site [1]. Models of the same type have been used to describe tunneling through a magnetic impurity connected to two perfect leads in the presence of a magnetic field [2]. Another wide domain of application is the one of nonlinear optics. The type of system thereby considered is an array of coupled waveguides consisting of (at least) two types of materials one linear and one of Kerr type, see e.g. [3]. Several problems have been addressed, ranging from the existence of localized solutions residing on the nonlinear portion (nonlinear impurity modes [4]) to the scattering and transmission of plane waves through it [5]. A model which is often used to describe such a wide palette of problems is the discrete nonlinear Schrödinger equation. There, the discretization of the continuum Schrödinger operator is emulated by a predominant nearest-neighbor interaction. As is known, the seminal works of Davydov [6] and Holstein [7] were an early stimulus yielding a considerable body of work on discrete solitary waves (by pioneers such as Bishop, Campbell, Scott, and others); see e.g. the more recent account of [8]. Genuine nonlinear features, like the self-trapping transitions, are already present in few-degrees-of-freedom system, like for instance the dimer [9]. Early on in this literature, problems with one or multiple defect nodes embedded in linear chains were considered, see e.g. the work of [10, 11] and references therein.

An important question concerns the spectral characteristics of the problem in the linear regime and the dynamical

stability of the solutions in the nonlinear regime (i.e., when the embedded impurities are genuinely nonlinear). To the best of our knowledge no systematic study of such an important issue has been presented in the literature. In Ref. [12] the continuum case of Nonlinear Schrödinger equation with a localized (δ -function) nonlinearity was considered. For discrete lattices, similar techniques have been used to match an ansatz on the linear part of the lattice with the relevant Schrödinger equation condition on the nonlinear site(s) [13–15]. In [13, 16] “hot spot” sites carrying linear gain and cubic nonlinearity on an infinite lattice were investigated within a lossy bulk medium. An analysis of a related problem, the nonlinear Fano effect, has been reported in [17] (see also references therein). Another related reference is [18] where a bifurcation analysis of an open chain with nonlinearity and disorder is performed.

The aim of the present paper is to formulate (in general) and to solve (in some specific cases) the spectral problem for a discrete Schrödinger equation with $N \geq 2$ embedded defects (an N -site oligomer [19]). Equations of this type emerge in, at least, two interesting cases. The first is the one of linear chains with localized *complex* on-site potentials. The second one arises when considering the stability problem of complex (i.e. current carrying) scattering solutions of the discrete nonlinear Schrödinger equation [5]. Such solutions can be computed exactly by the transfer matrix method [5, 20–22] and linearization around them yields linear equations of the same type.

Our motivation to approach this issue is twofold. The first is to study the scattering problem by open systems possessing a \mathcal{PT} -symmetry [23–25]. This theme is rapidly evolving into a major area of research partly due to its providing an intriguing alternative set of non-Hermitian Hamiltonians with potentially real eigenvalues and partly due to its experimental realizations in the field of nonlinear optics, both in the case of dimers [26, 27] and even in that of whole lattices [28]. The second motivation stems from a recent study of non-reciprocal wave propagation through non-mirror symmetric nonlinear lattices [29]. These are a minimal model for a “wave diode”, namely for devices capable to selectively rectify wave energy through a nonlinear medium of propagation. Relevant applications arise for instance for phonon scattering at a nonlinear interface layer between two very dissimilar crystals [30], acoustic waves in sonic materials [31] or in the so-called all-optical diode for photonic applications [32].

The solution of infinite-dimensional problems like the above is technically more involved than a straightforward matrix diagonalization. Indeed, to solve the problem exactly one should impose the solution a definite plane wave form (with generally complex wave numbers) in the two semi-infinite linear parts of the chain. The matching of such waves through the oligomer portion reduces the infinite-dimensional problem to an homogeneous linear system of $2N$ equations, whose solvability condition, along with the dispersion relations, yields a set of nonlinear equations for the unknowns. We characterize our method as “semi-analytic”, namely it is exact yet it relies on numerical solutions of a high degree polynomial equation. As a relevant disclaimer here, we should point out that our method is not proposed as an advantageous computational alternative to standard full eigenvalue solvers. Instead, our results are intended to give mathematical form and physical understanding, as close to analytic as is possible, to the output of an otherwise purely numerical computation. For instance, the process provides insight on the functional form of the corresponding eigenvectors.

The details of this method will be presented for a linear \mathcal{PT} -symmetric case [23–25]. In the latter, the imposition of the parity (\mathcal{P} , associated with spatial reflection) and time-reversal (\mathcal{T} , associated with temporal reflection and also $i \rightarrow -i$) symmetries leads to an imaginary (growth/decay) part of the Schrödinger potential which is spatially odd. The relevant more general constraint, in fact, reads $V(x) = V^*(-x)$ (where \star stands for complex conjugation); i.e., the real part of the relevant potential needs to be even. This setting will be compared/contrasted to the Hamiltonian case, where the potential is real.

The paper is organized as follows. In section II, we will discuss the simplest case namely that of linear oligomers. Although simple, this case is useful to set the stage of the general methodology and to illustrate some basic features that will be useful throughout the rest of the paper. In section III, we turn to the nonlinear case. In each of these, we first present the relevant analysis and subsequently we corroborate it on the basis of numerical computations. Finally, in section IV, we present a summary of our findings and some potential directions for future study.

II. LINEAR CASE

In this section we present the strategy to compute the spectrum and eigenstates of a general linear problem where N -site complex defects are embedded in an otherwise homogeneous lattice. More precisely, we consider the dynamic evolution of a one-dimensional chain governed by the linear discrete Schrödinger equation

$$i\dot{\phi}_n - V_n\phi_n + \phi_{n+1} + \phi_{n-1} = 0 \quad (1)$$

where $\phi_n(t) \in \mathbb{C}$. The complex potential $V_n \in \mathbb{C}$ is zero everywhere except for $1 \leq n \leq N$ for some integer $N \geq 2$.

We look for solutions of the form $\phi_n(t) = a_n e^{i\omega t}$ so that (1) becomes the time-independent condition

$$a_{n+1} + a_{n-1} - (V_n + \omega)a_n = 0. \quad (2)$$

Note that a_n is complex as well.

A. Theoretical Analysis

Our goal is to present a strategy for the analytic computation of the eigenstates a_n and eigenvalues ω , assuming that V_n has been prescribed. First we begin with an observation which applies to the portions of the lattice on the left and right of the N central sites. The zero potential ($V_n = 0$) version of equation (2) has a general solution of the form $a_n = Ae^{i\kappa n} + Be^{-i\kappa n}$ for $A, B \in \mathbb{C}$ and $\kappa \in \mathbb{C}$ satisfying the dispersion relation $2 \cos(\kappa) = \omega$. Thus we begin with the ansatz

$$a_n = \begin{cases} Ae^{i\kappa n} + Be^{-i\kappa n} & n < 1 \\ Ce^{i\kappa n} + De^{-i\kappa n} & n > N \end{cases} \quad (3)$$

for $A, C, B, D \in \mathbb{C}$ and κ satisfying

$$\omega = z + \frac{1}{z} \quad (4)$$

where we use the shorthand notation $z = e^{i\kappa} \neq 0$. Imposing (3) and (4) is enough to satisfy (2) for all n except $n = 0, 1, \dots, N, N + 1$. Applying (3) to (2) with $n = 0, N + 1$ shows that the formula (3) is applicable at $n = 1, N$. Since in practice we deal with a finite length lattice we introduce indexing $n_0 \leq n \leq m_0$ for large magnitude integers $n_0 \ll 1$ and $m_0 \gg N$. Imposing [38] homogeneous Dirichlet boundary conditions $a_{n_0-1} = a_{m_0+1} = 0$ shows that $\omega = a_{n_0+1}/a_{n_0} = a_{m_0-1}/a_{m_0}$. Combining this with (3) gives $B = -Ae^{2i\kappa(n_0-1)}$ and $D = -Ce^{2i\kappa(m_0+1)}$. Thus we have

$$a_n = \begin{cases} Ac_n & n \leq 1 \\ Cd_n & n \geq N \end{cases} \quad (5)$$

for $c_n = z^n - z^{2n_0-2-n}$ and $d_n = z^n - z^{2m_0+2-n}$.

At this point the imposition of (5) and (4) is enough to satisfy all but the N equations in (2) with $n = 1, \dots, N$. In the following sections we outline strategies for completing the computation of a_n and ω in the cases of embedded few-site defects and apply the method to our \mathcal{PT} -symmetric or Hamiltonian oligomer.

1. Oligomer of length two

For $N = 2$ we examine the two equations (2) for $n = 1, 2$ which by (5) can be written as

$$P \begin{bmatrix} a_0 \\ a_1 \\ a_2 \\ a_3 \end{bmatrix} = PQ \begin{bmatrix} A \\ C \end{bmatrix} = 0 \quad \text{for} \quad P = \begin{bmatrix} 1 & -(V_1 + \omega) & 1 & 0 \\ 0 & 1 & -(V_2 + \omega) & 1 \end{bmatrix} \quad \text{and} \quad Q = \begin{bmatrix} c_0 & 0 \\ c_1 & 0 \\ 0 & d_2 \\ 0 & d_3 \end{bmatrix}. \quad (6)$$

In other words, we now have a 2×2 system with unknowns A, C and coefficient matrix PQ . Imposing zero determinant $\det(PQ) = 0$ gives a solvability condition, which by (4) amounts to requiring that allowable z are roots of a polynomial with coefficients in terms of V_n . For each root z one computes the corresponding A, C by the equation in (6) so that finally an eigenvalue ω and eigenvector a_n are known by (4) and (5). Note that roots $z = \pm 1$ correspond to $c_n = d_n = a_n = 0$ and should be disregarded so as to obtain non-trivial eigenvectors.

As an example, consider the special case $V_1 + V_2 = 0$. One can compute by hand that the determinant condition, when expressed in terms of a positive power polynomial, is

$$0 = z^{2(m_0-n_0)+6} + (V_1V_2 - 1)z^{2(m_0-n_0)+4} - V_1z^{2m_0+1} - V_1V_2z^{2m_0} - V_2z^{2m_0-1} - V_2z^{-2n_0+7} - V_1V_2z^{-2n_0+6} - V_1z^{-2n_0+5} + (V_1V_2 - 1)z^2 + 1 \quad (7)$$

for which $z = \pm 1$ are each double roots. This reduces the number of relevant roots of (7) to $2(m_0 - n_0 + 1) \equiv 2L$, twice the length of the lattice. One can easily show, using the symmetry of the coefficients in (7), that solutions of (7) occur in reciprocal pairs $z, \frac{1}{z}$. Combining this with (4) shows that our analytic computation indeed yields exactly L eigenvalues ω , counted with multiplicity.

2. Oligomer of length three or greater

For $N > 2$ the strategy is similar to that of the last section but involves an additional step. First focus on the $N - 2$ equations (2) for $n = 2, \dots, N - 1$ which we write as

$$\begin{bmatrix} 1 & -(V_2 + \omega) & 1 & & & \\ & \ddots & \ddots & \ddots & & \\ & & & 1 & -(V_{N-1} + \omega) & 1 \end{bmatrix} \begin{bmatrix} a_1 \\ \vdots \\ a_N \end{bmatrix} = 0. \quad (8)$$

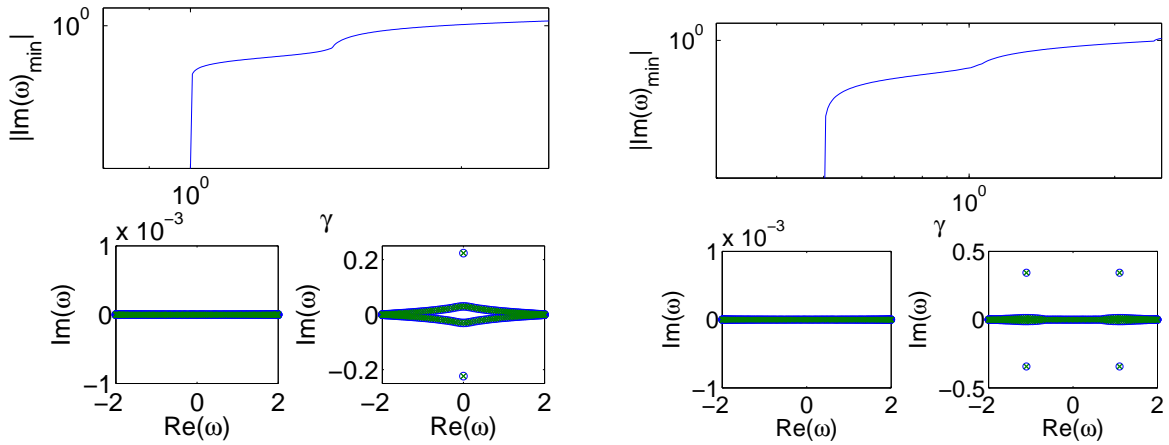


FIG. 1: The left set of panels corresponds to the linear \mathcal{PT} -symmetric dimer with $N = 2$ and $V_1 = i\gamma = -V_2$ while the right set of panels to the case of the trimer with $N = 3$ and $V_1 = i\gamma = -V_3, V_2 = 0$. Each set contains a (top) plot of linear stability eigenfrequencies as a function of increasing γ as computed on a lattice of length 200. The eigenvalue agreement between numeric (circles) and exact (x's) computations is shown for $\gamma = .5$ (bottom left) and $\gamma = 1.5$ (bottom right).

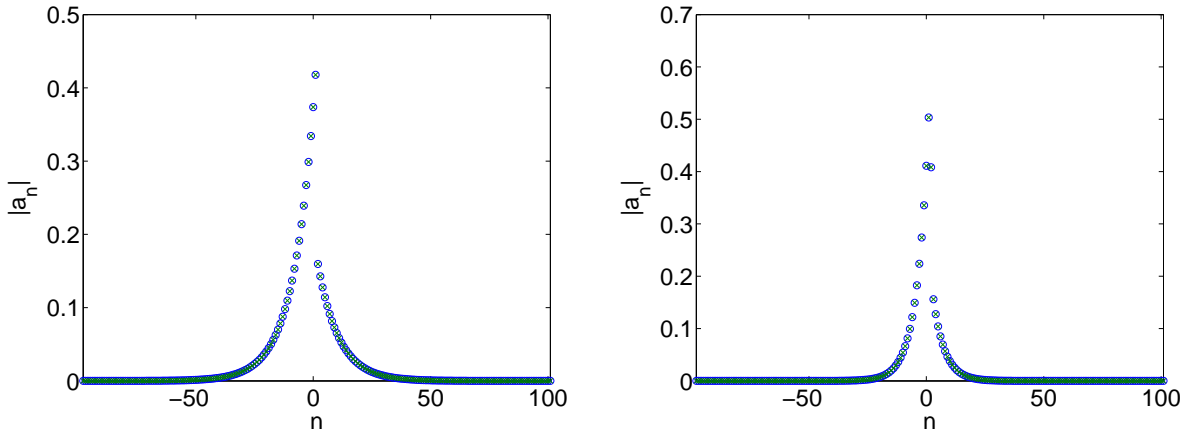


FIG. 2: Profiles of modulus of unstable eigenvectors $|a_n|$ are shown for the linear dimer (left) and the linear trimer (right). These eigenvectors correspond to the eigenvalues with negative imaginary part for $\gamma = 1.5$ which are seen in the bottom right panels of Fig. 1. Again, numerical computations (circles) are shown to agree with the exact computation (x's) and the lattice length is 200.

By moving a_1 in the first equation and a_N in the last equation to the right-hand-side, (8) can be written as a square $(N - 2) \times (N - 2)$ system with unknowns a_2, \dots, a_{N-1} that can be computed linearly in terms of a_1, a_N (under appropriate conditions of invertibility of the resulting coefficient matrix). For the case of $N = 3$, Eq. (8) is one equation which we solve for a_2 in terms of a_1, a_3 to obtain

$$a_2 = \frac{a_1 + a_3}{V_2 + \omega} \stackrel{\text{by (5)}}{=} \frac{c_1 A + d_3 C}{V_2 + \omega} \quad (9)$$

for $\omega \neq -V_2$.

Continuing with the $N = 3$ case, we use (5) and (9) to rewrite the two remaining equations in (2) with $n = 1, 3$ as

$$P \begin{bmatrix} a_0 \\ a_1 \\ a_2 \\ a_3 \\ a_4 \end{bmatrix} = PQ \begin{bmatrix} A \\ C \end{bmatrix} = 0 \quad \text{for} \quad P = \begin{bmatrix} 1 & -(V_1 + \omega) & 1 & 0 & 0 \\ 0 & 0 & 1 & -(V_3 + \omega) & 1 \end{bmatrix} \quad \text{and} \quad Q = \begin{bmatrix} c_0 & 0 \\ c_1 & 0 \\ \frac{c_1}{V_2 + \omega} & \frac{d_3}{V_2 + \omega} \\ 0 & d_3 \\ 0 & d_4 \end{bmatrix}. \quad (10)$$

Again the solvability condition is $\det(PQ) = 0$ so that z is a root of a polynomial with coefficients in terms of V_n . For each z , one computes A, C in the nullspace of PQ from (10) so that by (4), (5) and (9), an eigenvalue ω and the

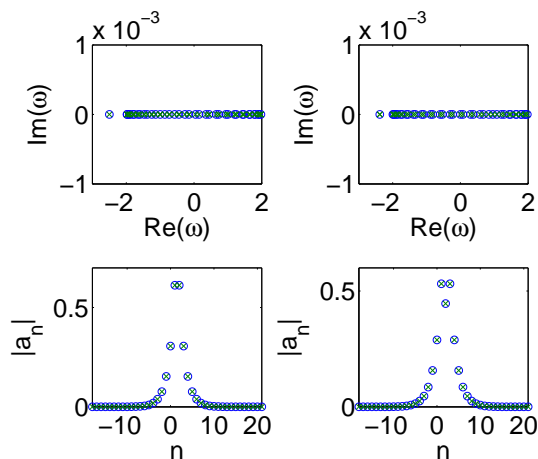


FIG. 3: The left set of plots corresponds to the linear Hamiltonian dimer with $N = 2$ and $V_1 = 1 = V_2$ while the right set of plots to the case of the linear trimer with $N = 3$ and $V_1 = 1 = V_3, V_2 = 0$. Each set contains a (top) plot of linear stability eigenvalues and a (bottom) plot of the eigenvector for the defect (point spectrum) mode. All plots show agreement between the numerical (circles) and semi-analytical (x's) results. Here the lattice length is 40.

corresponding eigenvector a_n are obtained. The $N > 3$ case is similar in that P and Q are determined using (5) and the above described process of using (8) to obtain expressions for a_2, \dots, a_{N-1} in terms of A, C .

Due to the condition obtained in (9), if there exists an eigenvalue $\omega = -V_2$ then it will not be found by the above process. In the case that such an eigenvalue exists the corresponding eigenvector is found by using (5) to rewrite the three $n = 1, 2, 3$ equations in (2) as the 2×2 system

$$\begin{bmatrix} (V_1 - V_2)c_1 - c_0 & (V_2 - V_3)d_3 + d_4 \\ c_1 & d_3 \end{bmatrix} \begin{bmatrix} A \\ C \end{bmatrix} = 0 \quad (11)$$

for z such that $z + \frac{1}{z} = -V_2$. Then a_n is computed by (5) and $a_2 = (V_1 - V_2)a_1 - a_0 = (V_3 - V_2)a_3 - a_4$.

B. Numerical results

First, we focus on the \mathcal{PT} -symmetric case where the dimer has linear potential $V_1 = -V_2 = i\gamma$ and the trimer potential is $V_1 = -V_3 = i\gamma$, while $V_2 = 0$. Fig. 1 shows agreement between the eigenvalues ω computed numerically directly from (2), through an eigenvalue solver, as compared to the semi-analytic calculation involving the identification of the roots of an equation of the form of Eq. (7), as outlined in the above theoretical analysis section. Fig. 2 shows the accuracy of the semi-analytic calculation in predicting the modulus profile of the eigenvectors $|a_n|$.

The spectra in Fig. 1 have both, as expected, a continuum component filling densely the interval $[-2, 2]$ on the real axis corresponding to the propagation of linear waves. For $\gamma > \gamma_c$ the solutions become unstable [39]; this is the so-called \mathcal{PT} -phase transition of [23–25]. In the case of the dimer, the principal unstable eigenfrequency pair has zero real part and is purely imaginary. In the case of the trimer, on the other hand, there is some oscillatory behaviour superimposed to the exponential growth of perturbations. The exponential localization of the associated eigenvectors is associated with the localized nature of the embedded defect structure and is showcased in Fig. 2.

Finally, as regards the linear eigenvalue problem, we consider the Hamiltonian case where the dimer has a linear potential $V_1 = V_0(1 + \delta)$, $V_2 = V_0(1 - \delta)$ and the trimer potential is $V_1 = V_0(1 + \delta)$, $V_2 = 0$, $V_3 = V_0(1 - \delta)$. Fig. 3 shows agreement between the numerically computed and semi-analytically calculated eigenvalues and the (modulus of the localized) eigenvectors. A fundamental difference here concerns the Hermitian nature of the relevant (matrix) operator which excludes the possibility of imaginary eigenfrequencies. Nevertheless, there exists within the spectrum a real defect eigenvalue. For $\delta > 0$, this frequency decreases as δ increases and the corresponding eigenvector profiles for $\delta > 0$ are typically similar to what is seen in Fig. 3.

III. NONLINEAR CASE

Let us now consider the nonlinear Schrödinger equation [33]

$$i\dot{\Phi}_n - V_n\Phi_n + \Phi_{n+1} + \Phi_{n-1} = \alpha_n|\Phi_n|^2\Phi_n \quad (12)$$

for $\alpha_n \in \mathbb{R}$ zero everywhere except $1 \leq n \leq N$. Seeking, as is customary, stationary solutions of the form $\Phi_n(t) = \psi_n e^{-i\omega t}$, we find that they should satisfy

$$\omega\psi_n - V_n\psi_n + \psi_{n+1} + \psi_{n-1} = \alpha_n|\psi_n|^2\psi_n. \quad (13)$$

We consider the dynamics of small perturbations defined by

$$\Phi_n(t) = (\psi_n + \epsilon\phi_n)e^{-i\omega t}; \quad \phi_n \equiv \left(a_n e^{i\nu t} + b_n e^{-i\nu^* t} \right) \quad (14)$$

for $\omega \in \mathbb{R}$ and $a_n, b_n, \nu \in \mathbb{C}$ and with $\psi_n \in \mathbb{C}$. In order to investigate the stability, we examine the resulting order- ϵ equations, amounting to the spectral or linear stability analysis equations

$$i\dot{\phi}_n = (V_n - \omega)\phi_n - \phi_{n+1} - \phi_{n-1} + \alpha_n (2|\psi_n|^2\phi_n + \psi_n^2\phi_n^*). \quad (15)$$

Note that ϕ_n is complex. It is thus recognized that problem (15) is similar to (1), the main difference being that now ϕ_n is coupled to ϕ_n^* . Hence, given a zeroth-order solution ψ_n , we can apply a similar approach as the one developed in section II, in order to determine its linearization spectrum.

For later reference, it is convenient to reformulate the problem in matrix form for a_n, b_n which are obtained from (12) by equating coefficients of $e^{i(\nu-\omega)t}, e^{-i(\nu^*+\omega)t}$, yielding

$$\nu \begin{bmatrix} a_n \\ b_n^* \end{bmatrix} = F \begin{bmatrix} a_n \\ b_n^* \end{bmatrix} \quad (16)$$

for $F = \begin{bmatrix} F_1 & F_2 \\ F_3 & F_4 \end{bmatrix}$ and

$$\begin{aligned} F_1 &= \text{diag}(\omega - V_n - 2\alpha_n|\psi_n|^2) + G & F_2 &= -\text{diag}(\alpha_n\psi_n^2) \\ F_3 &= \text{diag}(\alpha_n(\psi_n^*)^2) & F_4 &= -\text{diag}(\omega - V_n^* - 2\alpha_n|\psi_n|^2) - G \end{aligned} \quad (17)$$

where G is a sparse matrix with ones on the first super- and sub-diagonal.

A. Theoretical Analysis

Similar to the linear case we begin with the linearization problem ansatz

$$a_n = \begin{cases} Ae^{i\kappa n} + Be^{-i\kappa n} & n < 1 \\ Ce^{i\kappa n} + De^{-i\kappa n} & n > N \end{cases}, \quad b_n^* = \begin{cases} A'e^{i\kappa' n} + B'e^{-i\kappa' n} & n < 1 \\ C'e^{i\kappa' n} + D'e^{-i\kappa' n} & n > N \end{cases} \quad (18)$$

for $A, C, B, D, A', C', B', D' \in \mathbb{C}$ and $\kappa, \kappa' \in \mathbb{C}$ satisfying dispersion relations

$$\nu - \omega = 2 \cos(\kappa) \quad -(\nu + \omega) = 2 \cos(\kappa'). \quad (19)$$

Imposing (18) and (19) is enough to satisfy all equations in (16) except those with $n = 0, 1, \dots, N, N+1$. Applying (18) to (16) also shows that formulae (18) are applicable at $n = 1, N$. Homogeneous Dirichlet boundary conditions $a_{n_0-1} = b_{n_0-1}^* = a_{m_0+1} = b_{m_0+1}^* = 0$ (again for simplicity/specificity) imply that $\nu - \omega = a_{n_0+1}/a_{n_0} = a_{m_0-1}/a_{m_0}$ and $-(\nu + \omega) = b_{n_0+1}^*/b_{n_0}^* = b_{m_0-1}^*/b_{m_0}^*$ which when combined with the ansatz (18) gives $B = -Ae^{i\kappa(2n_0-2)}$, $D = -Ce^{i\kappa(2m_0+2)}$, $B' = -A'e^{i\kappa'(2n_0-2)}$, $D' = -C'e^{i\kappa'(2m_0+2)}$. Thus we have

$$a_n = \begin{cases} Ac_n & n \leq 1 \\ Cd_n & n \geq N \end{cases}, \quad b_n^* = \begin{cases} A'c'_n & n \leq 1 \\ C'd'_n & n \geq N \end{cases} \quad (20)$$

where c_n is defined in terms of $z = e^{i\kappa}$ as before and $c'_n = (z')^n - (z')^{2n_0-2-n}$, $d'_n = (z')^n - (z')^{2m_0+2-n}$ for $z' = e^{i\kappa'}$.

When combined with the dispersion relations (19), the condition (20) is enough to satisfy all except the $2N$ equations in (16) associated with $n = 1, \dots, N$. Again we separate the remaining parts of the computation into two sections.

1. Oligomer of length two

For $N = 2$ the remaining four equations in (16) for $n = 1, 2$ can be written as $Pv = 0$ for $P = \begin{pmatrix} P_1 & P_2 \\ P_3 & P_4 \end{pmatrix}$ and

$$P_1 = \begin{bmatrix} 1 & \omega - \nu - V_1 - 2\alpha_1|\psi_1|^2 & 1 & 0 \\ 0 & 1 & \omega - \nu - V_2 - 2\alpha_2|\psi_2|^2 & 1 \end{bmatrix}, \quad P_2 = \begin{bmatrix} 0 & -\alpha_1\psi_1^2 & 0 & 0 \\ 0 & 0 & -\alpha_2\psi_2^2 & 0 \end{bmatrix},$$

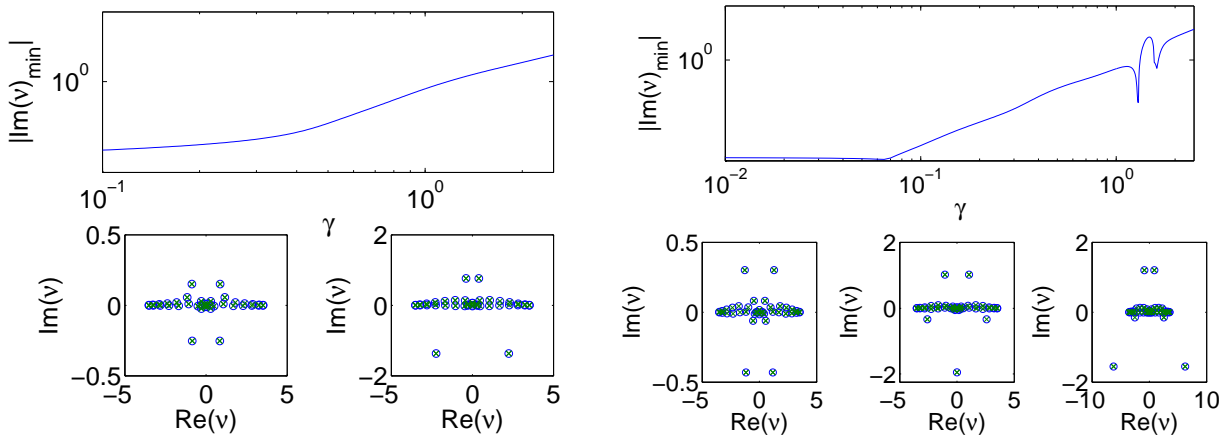


FIG. 4: The left set of panels corresponds to the \mathcal{PT} -symmetric dimer with $N = 2$, $\alpha_{1,2} = 1$ and $V_1 = i\gamma = -V_2$ while the right set of panels to the case of the trimer with $N = 3$, $\alpha_{1,2,3} = 1$ and $V_1 = i\gamma = -V_3, V_2 = 0$. Each set contains a (top) plot of linear stability eigenfrequencies of the stationary solution corresponding to $T = 0.7$ and $k_0 = 2.5$ as computed on a lattice of length 20. Plots of the eigenvalue ν indicating agreement between numeric (circles) and exact (x's) results are shown for the dimer with $\gamma = .5$ (bottom left) and $\gamma = 1.5$ (bottom right), and for the trimer with $\gamma = .5$ (bottom left) and $\gamma = 1.5$ (bottom middle) and $\gamma = 1.75$ (bottom right). For the trimer, when γ is small the dominant pair of (unstable) eigenfrequencies of negative imaginary part increases in magnitude as γ increases until $\gamma \approx 1.15$. At this point the complex pair recedes and a single dominant purely imaginary emerges at $\gamma \approx 1.3$. This single eigenfrequency increases in magnitude until $\gamma \approx 1.49$ when it begins to decrease. At $\gamma \approx 1.62$, a new dominant complex pair increases in magnitude and continues to increase as γ increases.

(21)

$$P_3 = \begin{bmatrix} 0 & \alpha_1 (\psi_1^*)^2 & 0 & 0 \\ 0 & 0 & \alpha_2 (\psi_2^*)^2 & 0 \end{bmatrix}, \quad P_4 = \begin{bmatrix} -1 & -\omega - \nu + V_1^* + 2\alpha_1 |\psi_1|^2 & -1 & 0 \\ 0 & -1 & -\omega - \nu + V_2^* + 2\alpha_2 |\psi_2|^2 & -1 \end{bmatrix},$$

where $v = \begin{bmatrix} a_n \\ b_n^* \end{bmatrix}$ is a vector of length eight with each of a_n, b_n^* restricted to the index $0 \leq n \leq 3$. By (20), v can be written as

$$v = Q \begin{bmatrix} A \\ C \\ A' \\ C' \end{bmatrix} \quad \text{for} \quad Q = \begin{bmatrix} c_0 & 0 & 0 & 0 \\ c_1 & 0 & 0 & 0 \\ 0 & d_2 & 0 & 0 \\ 0 & d_3 & 0 & 0 \\ 0 & 0 & c'_0 & 0 \\ 0 & 0 & c'_1 & 0 \\ 0 & 0 & 0 & d'_2 \\ 0 & 0 & 0 & d'_3 \end{bmatrix}. \quad (22)$$

The solvability condition is then the pair of equations

$$\det(PQ) = 0, \quad z + \frac{1}{z} + \omega = - \left(z' + \frac{1}{z'} + \omega \right) \quad (23)$$

where the second was obtained from the dispersion relations (19). Solutions of (23) where either of z or z' is ± 1 can be disregarded since the resulting system $Pv = 0$ has no non-trivial solutions. The remaining solutions appear in quadruple sets $(z, z'), (z, \frac{1}{z'}), (\frac{1}{z}, z'), (\frac{1}{z}, \frac{1}{z'})$ so that the total number of relevant solutions of (23) is four times the length of the lattice. Thus by (19) the calculation yields a number (counted with algebraic multiplicity) of eigenvalues ν equal to the length of the lattice.

2. Oligomer of length three or greater

Similarly to the strategy for the linear case, for $N > 2$ we begin by examining the $2(N - 2)$ equations in (16) with $n = 2, \dots, N - 1$. Using (20) to rewrite the four quantities a_1, a_N, b_1^*, b_N^* one obtains a non-homogeneous

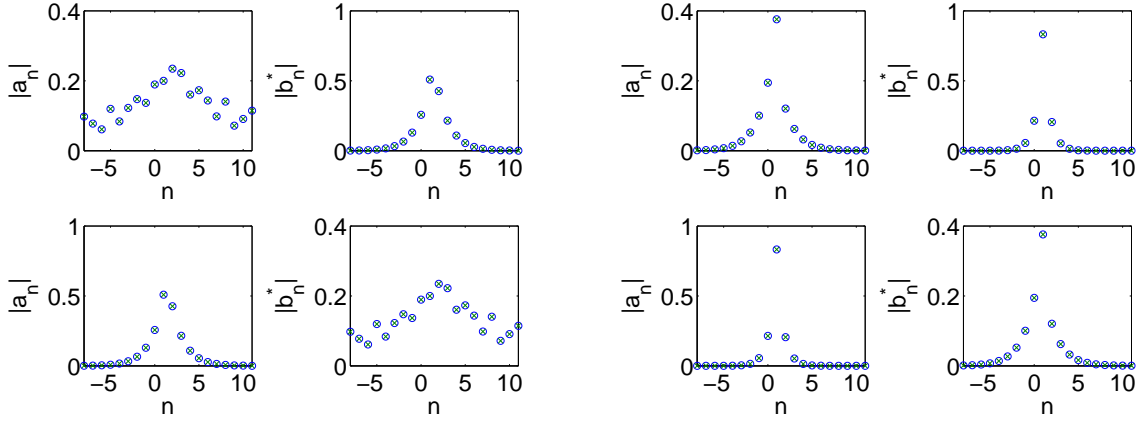


FIG. 5: Profiles of the moduli of unstable eigenvectors $|a_n|$, $|b_n^*|$ are shown for the nonlinear dimer. The left four plots show eigenvectors for $\gamma = .5$ and the right four plots for $\gamma = 1.5$. These eigenvectors correspond to eigenvalues with negative imaginary part which are seen in Fig. 4. Again, numerical computations are shown to agree with the exact (x's) results and the length of the lattice is 20. Notice the localization in both components of the eigenvector in the case of the \mathcal{PT} -symmetry breaking case of $\gamma > 1$.

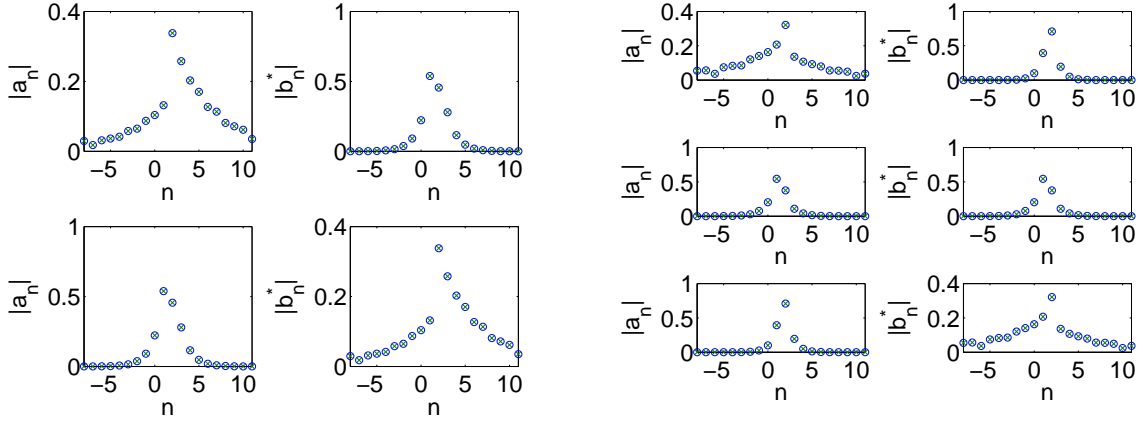


FIG. 6: Profiles of the moduli of unstable eigenvectors $|a_n|$, $|b_n^*|$ are shown for the nonlinear trimer with lattice length 20. The left four plots show eigenvectors for $\gamma = .5$ and the right six plots for $\gamma = 1.5$. These eigenvectors correspond to eigenvalues with negative imaginary part which are seen in Fig. 4. The agreement is similar to those of the earlier figures.

square system where the $2(N-2)$ variables $a_2, \dots, a_{N-1}, b_2^*, \dots, b_{N-1}^*$ can be computed as linear combinations of A, C, A', C' , under appropriate conditions of invertibility of the coefficient matrix.

In the case of $N = 3$ the $2(N-2) = 2$ equations can be written as

$$\begin{bmatrix} 1 & \omega - \nu - V_2 - 2\alpha_2|\psi_2|^2 & 1 & 0 & -\alpha_2\psi_2^2 & 0 \\ 0 & \alpha_2(\psi_2^*)^2 & 0 & -1 & -\omega - \nu + V_2^* + 2\alpha_2|\psi_2|^2 & -1 \end{bmatrix} \begin{bmatrix} a_n \\ b_n^* \end{bmatrix} = 0 \quad (24)$$

where the column vector is length six with $1 \leq n \leq 3$. We move a_1, a_3, b_1^*, b_3^* to the right-hand-side of (24) and use (20) to obtain

$$\begin{bmatrix} a_2 \\ b_2^* \end{bmatrix} = M \begin{bmatrix} A \\ C \\ A' \\ C' \end{bmatrix} \quad \text{for} \quad M = \begin{bmatrix} \omega - \nu - V_2 - 2\alpha_2|\psi_2|^2 & -\alpha_2\psi_2^2 \\ \alpha_2(\psi_2^*)^2 & -\omega - \nu + V_2^* + 2\alpha_2|\psi_2|^2 \end{bmatrix}^{-1} \begin{bmatrix} -c_1 & -d_3 & 0 & 0 \\ 0 & 0 & c'_1 & d'_3 \end{bmatrix}. \quad (25)$$

Of course, (25) is the nonlinear analogue of (9) and the values of z which are found by the remaining parts of the computation are such that the inverse matrix in (25) exists. The four remaining equations in (16) with $n = 1, 3$ can

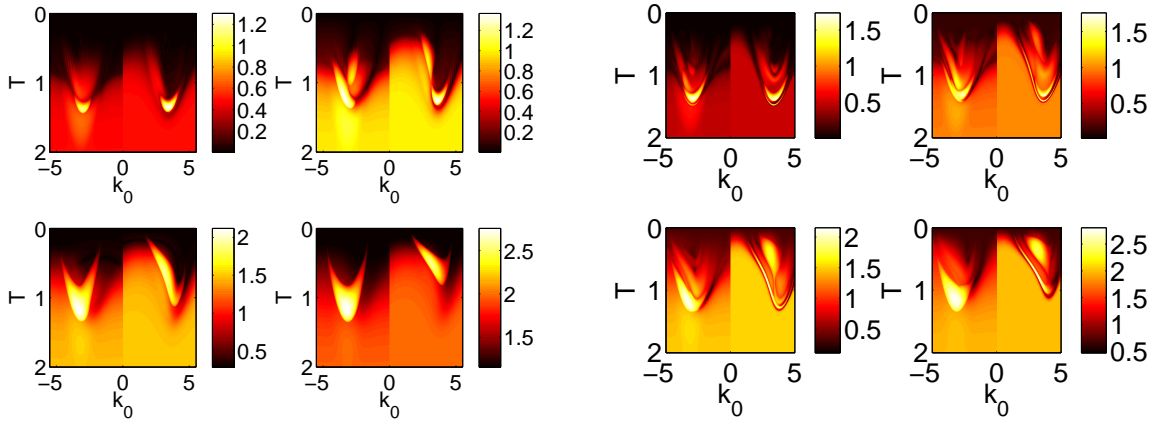


FIG. 7: The left set of panels correspond to the \mathcal{PT} -symmetric dimer with $N = 2$, $\alpha_{1,2} = 1$ and $V_1 = i\gamma = -V_2$ while the right set of panels to the case of the trimer with $N = 3$, $\alpha_{1,2,3} = 1$ and $V_1 = i\gamma = -V_3, V_2 = 0$. Each set contains contour plots of extremal stability eigenfrequencies $|Im(\nu)_{min}|$ for extended solutions as in (28) on a lattice of length 20 with $\gamma = .5$ (top left), $\gamma = 1$ (top right), $\gamma = 1.5$ (bottom left) and $\gamma = 2$ (bottom right).

now be written as $Pv = 0$ for $P = \begin{pmatrix} P_1 & P_2 \\ P_3 & P_4 \end{pmatrix}$ with

$$P_1 = \begin{bmatrix} 1 & \omega - \nu - V_1 - 2\alpha_1|\psi_1|^2 & 1 & 0 \\ 0 & 0 & 1 & \omega - \nu - V_3 - 2\alpha_3|\psi_3|^2 & 1 \end{bmatrix}, \quad P_2 = \begin{bmatrix} 0 & -\alpha_1\psi_1^2 & 0 & 0 & 0 \\ 0 & 0 & 0 & -\alpha_3\psi_3^2 & 0 \end{bmatrix} \quad (26)$$

$$P_3 = \begin{bmatrix} 0 & \alpha_1(\psi_1^*)^2 & 0 & 0 & 0 \\ 0 & 0 & 0 & \alpha_3(\psi_3^*)^2 & 0 \end{bmatrix}, \quad P_4 = \begin{bmatrix} -1 & -\omega - \nu + V_1^* + 2\alpha_1|\psi_1|^2 & -1 & 0 \\ 0 & 0 & 0 & -1 & -\omega - \nu + V_3^* + 2\alpha_3|\psi_3|^2 & -1 \end{bmatrix}$$

and where $v = \begin{bmatrix} a_n \\ b_n^* \end{bmatrix}$ is length ten with $0 \leq n \leq 4$. By (20) and (25) we write

$$v = Q \begin{bmatrix} A \\ C \\ A' \\ C' \end{bmatrix} \quad \text{for} \quad Q = \begin{bmatrix} c_0 & 0 & 0 & 0 \\ c_1 & 0 & 0 & 0 \\ M_{11} & M_{12} & M_{13} & M_{14} \\ 0 & d_3 & 0 & 0 \\ 0 & d_4 & 0 & 0 \\ 0 & 0 & c'_0 & 0 \\ 0 & 0 & c'_1 & 0 \\ M_{21} & M_{22} & M_{23} & M_{24} \\ 0 & 0 & 0 & d'_3 \\ 0 & 0 & 0 & d'_4 \end{bmatrix}. \quad (27)$$

The solvability condition is the same as (23) but with P and Q as defined in (26) and (27), respectively. Again, solutions with either z or z' equal to ± 1 are not relevant.

B. Numerical results

As mentioned in the Introduction, one of the motivations of the present work is to study the stability of scattering solutions. In particular, we focus here on of the class of plane wave solutions of (13) of the form

$$\psi_n = \begin{cases} R_0 e^{ik_0 n} + R e^{-ik_0 n} & n \leq 1 \\ T e^{ik_0 n} & n \geq N \end{cases} \quad (28)$$

with $R_0, R, T \in \mathbb{C}$ representing the incident, reflected and transmitted amplitudes, respectively and $k_0 \geq 0$ is the wavenumber such that $\omega = -2 \cos(k_0)$. For each given values of k_0, T one can compute ψ_n by repeated application of the backwards transfer map [5, 20–22]

$$\psi_{n-1} = -\psi_{n+1} + (V_n - \omega + \alpha_n |\psi_n|^2) \psi_n \quad (29)$$

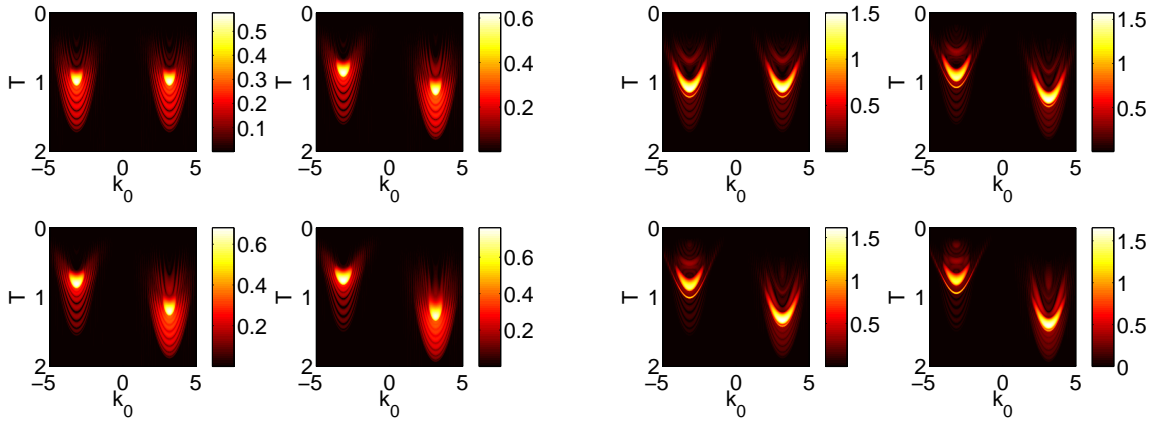


FIG. 8: The left set of panels correspond to the Hamiltonian dimer with $N = 2$, $\alpha_{1,2} = 1$ and $V_1 = 1 + \delta, V_2 = 1 - \delta$ while the right set of panels to the case of the trimer with $N = 3$, $\alpha_{1,2,3} = 1$ and $V_1 = 1 + \delta, V_2 = 0, V_3 = 1 - \delta$. Each set contains contour plots of extremal stability eigenfrequencies $|Im(\nu)_{min}|$ for extended solutions as in (28) on a lattice of length 20 with $\delta = 0$ (top left), $\delta = 0.5$ (top right), $\delta = 0.75$ (bottom left) and $\delta = 1$ (bottom right).

which is a rearrangement of (13). For short oligomers, like the ones we are dealing with here, the ψ_n can be evaluated analytically [29, 34].

Fig. 4 shows an example of the the eigenvalues ν computed with the method discussed in the previous section. As a check, we also report eigenvalues computed by numerical diagonalization of the matrix F in (16) evaluated by substituting the computed ψ_n in (17). The corresponding eigenvectors for the case of the dimer and the trimer are shown, respectively, in Figs. 5 and 6.

It is clear that past the critical point of the \mathcal{PT} phase transition, the relevant eigenvectors become highly localized (contrary to what is the case with the more spatially extended eigenvectors before the transition). These eigenvectors are responsible for the rapid growth of the norm density at the gain node observed previously [34]. The analysis also confirms the finding from our previous work [34] that higher values of γ and T correspond to more unstable solutions. We partially capture this phenomenon in Fig. 7, which contains a systematic two-parameter diagram of the dependence of the growth rate of the corresponding most unstable eigenstates. In addition to the stronger instability for higher T observed in the figure (and also for higher γ in Fig. 4), we observe the asymmetry of the relevant growth rate for transmission in the direction of positive vs. negative k_0 (as in [29, 34] we have adopted the convention that $-k_0$ labels a right-incoming solution with wavenumber k_0). Among these two directions, it is intuitively clear and numerically confirmed that larger growth rates are incurred for waves that first encounter the gain site. For a fixed γ , the transition from right-incoming ($-k_0 < 0$) to left-incoming ($k_0 > 0$) waves may be achieved computationally by allowing the wave number to stay positive and instead flipping the potential V_n from left to right. For the \mathcal{PT} case this amounts to a continuous change in k_0 and a discontinuous change in the fixed γ value from negative to positive. This explains the discontinuity apparent in Fig. 7.

Finally, we touch upon the Hamiltonian case namely the case of real-valued V_n for the nonlinear problem [29] [once again we use a dimer with $V_1 = V_0(1 + \delta), V_2 = V_0(1 - \delta)$ and a trimer with $V_1 = V_0(1 + \delta), V_2 = 0, V_3 = V_0(1 - \delta)$]. This is captured in Fig. 8. In the Hamiltonian case the instability for the dimer associated with the particular values $k_0 = 2.5$ and $T = 0.7$, for example, increases as δ increases from zero to $\delta \approx 1.35$ then the instability decreases for increasing δ . Additional oscillations appear in Figure 8 as an artifact of the short lattice length which we used to obtain the higher resolution with respect to the axes of Figure 8. These extra fluctuations disappear for the dimer as the length of the lattice becomes large. Nevertheless, the persistent characteristic corroborating the earlier work of [29] identified here concerns the asymmetry of transmission between incoming from the left ($k_0 > 0$) and from the right ($k_0 < 0$).

IV. CONCLUSIONS & FUTURE CHALLENGES

In this work, we have presented a methodology for addressing the spectral analysis of linear (or linearized) chains that possess an embedded oligomer defect. The technique, which draws a series of direct parallels with the approach used in [12], consists of the solution of the linear problem (with its boundary conditions) on the lattice in which the defect is embedded. Subsequently these two linear solutions (on the left and right of the defect) are used as boundary conditions of the embedded region. Nontrivial solutions require that the determinant of a suitably defined matrix vanishes, ultimately leading to a polynomial problem for the eigenvalue, of the form given by (23). For the dimer, the polynomial problem can be formulated explicitly, see Eq. 7. In the general case, the eigenvalues and eigenvectors

of the full problem are obtained by numerical solutions and, the approach can be regarded as “semi-analytic”. In terms of computational cost and efficiency, our approach is not proposed as an advantageous alternative to algorithms in which eigenstates are computed by a computer algebra system directly from the relevant matrix equation. Its main merit is that of being exact (in as far as its analytical formulation goes) and of providing an analytical intuition towards the form of the eigenvectors of relevance to the problem.

We have applied the approach to genuinely linear problems with embedded complex oligomers (Section II), and, in the second part of the paper, to solve the stability problem as it arises from linearization around (analytically known or numerically computed) extended solutions with an embedded nonlinear defect (section III). Finally, we calculated the spectrum and eigenstates in a number of cases of interest for \mathcal{PT} -symmetric and Hamiltonian potentials. Our semi-analytical approach shows excellent agreement with numeric computations of the spectrum.

One important conclusion that arises from the specific instances that we have considered above is that the instabilities found in the nonlinear cases are generically oscillatory, with unstable eigenvalues having a non zero real and imaginary part and thus leading to oscillatory growth. As intuitively expected, the unstable eigenvectors are exponentially localized around the defects, as only perturbations located on nonlinear sites can grow. The question, however, of the dynamical development of the instability and of the ultimate fate of such solutions is still in many respects open to more systematic studies. In the Hamiltonian case, there is numerical evidence that the instability leads to self-trapping of energy at the oligomer [35]. On the other hand, the dynamics of the \mathcal{PT} case is fundamentally different in the instability development, usually ending in an indefinite growth at the gain site [34].

As formulated, the approach is fairly general and applies to the spectral problem of arbitrary stationary solutions of finite segments embedded in linear chains. This is true not only in the more standard Hamiltonian case of structural defects that has been investigated even experimentally -as regards its defect states and their interaction with discrete solitons [36]-; it is also true more generally for the open \mathcal{PT} -symmetric system case considered herein. In the latter, experiments have recently tracked the dimer problem [27], although longer size oligomer problems have not been experimentally reported as of yet. An especially interesting generalization would be to extend the present approach to higher dimensional settings. A priori, the solution of the linear problem is available in this case as well, e.g. for a square defect. Yet the matching of the solutions from the four relevant directions in the two-dimensional case presents considerable challenges. Generalizing the approach for both linear and nonlinear problems in such a case would be a particularly interesting topic for future studies. Another interesting issue to examine, even in the one dimensional setting, is the effect of boundary size on the eigenvalues of the problem (especially, so the \mathcal{PT} -symmetric one). Both our earlier work [34] and that of others [37] have suggested interesting effects stemming from the finite size of the domain (and the associated boundary conditions) within which the embedded defect lies. Studying such effects and their scaling over the domain size would be another interesting direction for future work. Relevant themes are currently under consideration and will be reported in future publications.

-
- [1] G.P. Tsironis, M.I. Molina and D. Hennig, *Phys. Rev. E* **50**, 2365 (1994).
 - [2] M.I. Molina, H. Bahlouli *Phys. Lett. A* **284**, 87 (2002).
 - [3] K. Hizanidis, Y. Kominis and N.K. Efremidis, *Opt. Express* **16**, 18296 (2008).
 - [4] P. G. Kevrekidis, Yu. S. Kivshar, and A. S. Kovalev *Phys. Rev. E* **67**, 046604 (2003)
 - [5] G.P. Tsironis and D. Hennig. *Phys. Rep.*, **307**, 333 (1999).
 - [6] A. S. Davydov, *Solitons in Molecular Systems*, 2nd ed. (Reidel, Dordrecht, 1991).
 - [7] T. Holstein, *Ann. Phys. (N.Y.)* **8**, 325 (1959); see also e.g. G.D. Mahan, *Many-Particle Physics* (Plenum, New York, 1981).
 - [8] A. C. Scott, *Nonlinear science. Emergence and dynamics of coherent structures*. (Oxford University Press, Oxford, 2003).
 - [9] V. M. Kenkre and D. K. Campbell, *Phys. Rev. B* **34**, 49594961 (1986).
 - [10] M.I. Molina and G.P. Tsironis, *Phys. Rev. B* **47**, 15330 (1993).
 - [11] D. Chen, M.I. Molina, G.P. Tsironis, *J. Phys.: Condens. Matter* **5**, 8689 (1993).
 - [12] B. A. Malomed and M. Ya. Azbel. *Phys. Rev. B*, **47**, 10402–10406 (1993).
 - [13] B. A. Malomed, E. Ding, K. W. Chow and S. K. Lai, *Phys. Rev. E* **86**, 036608 (2012).
 - [14] V. A. Brazhnyi and B. A. Malomed, *Phys. Rev. A* **86** 013829 (2012).

- [15] V. A. Brazhnyi and B. A. Malomed, *Phys. Rev. A* **83** 053844 (2011).
- [16] C. H. Tsang, B. A. Malomed, C. K. Lam and K. W. Chow, *Eur. Phys. J. D* **59**, No. 1, 81-89 (2010).
- [17] A. E. Miroschnichenko. *Phys. Lett. A*, **373**, 3586, (2009).
- [18] S. Tietsche and A. Pikovsky. *Europhys. Lett.*, **84**:10006 (2008).
- [19] K. Li and P. G. Kevrekidis *Phys. Rev. E* **83**, 066608 (2011)
- [20] F. Delyon, Y.E. Lévy, and B. Souillard, *Phys. Rev. Lett.*, **57**, 2010–2013 (1986).
- [21] Y. Wan and CM Soukoulis, *Phys. Rev. A*, **41**, 800–809 (1990).
- [22] Q. Li, CT Chan, KM Ho, and C.M. Soukoulis, *Phys. Rev. B*, **53** 15577–15585, (1996).
- [23] C. M. Bender and S. Boettcher, *Phys. Rev. Lett.* **80**, 5243-5246 (1998).
- [24] C. M. Bender, S. Boettcher and P. N. Meisinger, *J. Math. Phys.* **40**, 2201-2209 (1999).
- [25] C. M. Bender, *Rep. Prog. Phys.* **70**, 947-1018 (2007).
- [26] A. Guo, G. J. Salamo, D. Duchesne, R. Morandotti, M. Volatier-Ravat, V. Aimez, G. A. Siviloglou, and D. N. Christodoulides, *Phys. Rev. Lett.* **103**, 093902 (2009).
- [27] C.E. Rüter, K.G. Makris, R. El-Ganainy, D.N. Christodoulides, M.Segev, and D. Kip, *Nature Physics* **6**, 192-195 (2010).
- [28] A. Regensburger, C. Bersch, M.-A. Miri, G. Onishchukov, D.N. Christodoulides and U. Peschel, *Nature* **488**, 167-171 (2012).
- [29] S. Lepri and G. Casati, *Phys. Rev. Lett.* **106**, 164101 (2011).
- [30] Yu. A. Kosevich, *Phys. Rev. B*, **52**, 1017 (1995).
- [31] N. Boechler, G. Theocharis and C. Daraio, *Nature Materials* **10**, 665 (2011).
- [32] M. Scalora, J. P. Dowling, C. M. Bowden, and M. J. Bloemer, *J. Appl. Phys.* **76**, 2023 (1994); M. D. Tocci, M. J. Bloemer, M. Scalora, J. P. Dowling, and C. M. Bowden, *Appl. Phys. Lett.* **66**, 2324 (1995).
- [33] P. G. Kevrekidis. *The Discrete Nonlinear Schrödinger Equation*. Springer Verlag, Berlin, 2009.
- [34] J. D’Ambroise, P.G. Kevrekidis, and S. Lepri. *J. Phys. A* **45**, 444012 (2012).
- [35] S. Lepri and G. Casati, preprint arXiv:1211.4996.
- [36] R. Morandotti, H. S. Eisenberg, D. Mandelik, Y. Silberberg, D. Modotto, M. Sorel, C. R. Stanley, and J. S. Aitchison, *Opt. Lett.* **28**, 834 (2003).
- [37] A.A. Sukhorukov, S.V. Dmitriev, S.V. Suchkov and Yu.S. Kivshar, *Opt. Lett.* **37**, 2148 (2012).
- [38] This imposition is for simplicity/specificity of the calculation; other boundary conditions can be treated in similar ways by applying them to the solution of Eq. (3), to obtain two conditions relating A , B , C and D .
- [39] It should be noted that $\gamma_c = 1$ for the pure dimer (not embedded on a lattice) and for the dimer embedded on a finite lattice. Remarkably, the case of a dimer embedded in the infinite lattice has a different $\gamma_c = \sqrt{2}$ (D.E. Pelinovsky, personal communication). However, as our aim herein is to analyze the finite lattice case, we do not focus on this aspect further in what follows.